

Discrete Flavour Groups, θ_{13} and Lepton Flavour Violation

Guido Altarelli ^{a,b)}, Ferruccio Feruglio ^{c)},
Luca Merlo ^{d,e)}, and Emmanuel Stamou ^{d,e,f)}

^{a)} Dipartimento di Fisica ‘E. Amaldi’, Università di Roma Tre,
INFN, Sezione di Roma Tre, I-00146 Rome, Italy

^{b)} CERN, Department of Physics, Theory Division,
CH-1211 Geneva 23, Switzerland

^{c)} Dipartimento di Fisica ‘G. Galilei’, Università di Padova
INFN, Sezione di Padova, Via Marzolo 8, I-35131 Padua, Italy

^{d)} Physik-Department, Technische Universität München,
James-Franck-Strasse, D-85748 Garching, Germany

^{e)} TUM Institute for Advanced Study, Technische Universität München,
Lichtenbergstrasse 2a, D-85748 Garching, Germany

^{f)} Excellence Cluster Universe, Technische Universität München,
Boltzmannstrasse 2, D-85748 Garching, Germany

E-mail: guido.altarelli@cern.ch, feruglio@pd.infn.it,
luca.merlo@ph.tum.de, emmanuel.stamou@ph.tum.de

Abstract

Discrete flavour groups have been studied in connection with special patterns of neutrino mixing suggested by the data, such as Tri-Bimaximal mixing (groups A_4 , S_4 ...) or Bi-Maximal mixing (group S_4 ...) etc. We review the predictions for $\sin \theta_{13}$ in a number of these models and confront them with the experimental measurements. We compare the performances of the different classes of models in this respect. We then consider, in a supersymmetric framework, the important implications of these flavour symmetries on lepton flavour violating processes, like $\mu \rightarrow e\gamma$ and similar processes. We discuss how the existing limits constrain these models, once their parameters are adjusted so as to optimize the agreement with the measured values of the mixing angles. In the simplified CMSSM context, adopted here just for indicative purposes, the small $\tan \beta$ range and heavy SUSY mass scales are favoured by lepton flavour violating processes, which makes it even more difficult to reproduce the reported muon $g - 2$ discrepancy.

Contents

1	Introduction	1
2	Models	5
2.1	A_4 Models	6
2.1.1	Typical A_4 Models	8
2.1.2	Special A_4 Models	9
2.2	S_4 Models	13
3	Lepton Flavour Violation	17
3.1	Mass Insertions from Local Operators	20
3.1.1	Typical A_4 Models	21
3.1.2	Special A_4 Models	22
3.1.3	S_4 Models	22
3.2	Mass Insertions from low-energy RGE	23
3.3	Mass Insertion from high-energy RGE	27
3.4	Correlation with the Muon $g - 2$	32
4	Conclusion	33
A	Expression of $a_{CC'}$	35

1 Introduction

Neutrino mixing [1–6] is important because it could in principle provide new clues for the understanding of the flavour problem. Even more so since the neutrino mixing angles show a pattern that is completely different than that of quark mixing. The bulk of the data on neutrino oscillations are well described in terms of three active neutrinos. By now all three mixing angles have been measured, although with different levels of accuracy (see Table 1 [7]; see also Ref. [8]). In particular, we now have firm experimental evidence for a non-vanishing value of the smallest angle θ_{13} and a rather precise determination of its range (see Table 2 [9–12]).

Models of neutrino mixing based on discrete flavour groups have received a lot of attention in recent years [14–19]. There are a number of special mixing patterns that have been studied in that context. The corresponding mixing matrices all have $\sin^2 \theta_{23} = 1/2$, $\sin^2 \theta_{13} = 0$, values that are good approximations to the data, and differ by the value of the solar angle $\sin^2 \theta_{12}$. The observed $\sin^2 \theta_{12}$, the best measured mixing angle, is very close, from below, to the so called Tri-Bimaximal (TB) value [20–24] of $\sin^2 \theta_{12} = 1/3$ (see Fig. 1). Alternatively, it is also very close, from above, to the Golden Ratio (GR) value [25–28] $\sin^2 \theta_{12} = \frac{1}{\sqrt{5}\phi} = \frac{2}{5+\sqrt{5}} \sim 0.276$, where $\phi = (1 + \sqrt{5})/2$ is the GR (for a different connection to the GR, see Refs. [29, 30]). On a different perspective, one has also considered models with Bi-Maximal (BM) mixing, where $\sin^2 \theta_{12} = 1/2$, i.e. also maximal, as the neutrino mixing matrix before diagonalization of charged leptons. This is in line with the well-known empirical observation that $\theta_{12} + \theta_C \sim \pi/4$, where θ_C is the Cabibbo

Δm_{sun}^2 (10^{-5} eV ²)	$7.54^{+0.26}_{-0.22}$
Δm_{atm}^2 (10^{-3} eV ²)	$2.43^{+0.06}_{-0.10}$ ($2.42^{+0.07}_{-0.11}$)
$\sin^2 \theta_{12}$	$0.307^{+0.018}_{-0.016}$
$\sin^2 \theta_{23}$	$0.386^{+0.024}_{-0.021}$ ($0.392^{+0.039}_{-0.022}$)
$\sin^2 \theta_{13}$	$0.0241^{+0.0025}_{-0.0025}$ ($0.0244^{+0.0023}_{-0.0025}$)
δ_{CP}/π	$1.08^{+0.28}_{-0.31}$ ($1.09^{+0.38}_{-0.26}$)

Table 1: Fits to neutrino oscillation data from Ref. [7]. The results for both the normal and the inverse (in the brackets) hierarchies are shown.

Quantity	$\sin^2 2\theta_{13}$	$\sin^2 \theta_{13}$
T2K [9]	$0.11^{+0.11}_{-0.05}$ ($0.14^{+0.12}_{-0.06}$)	$0.028^{+0.019}_{-0.024}$ ($0.036^{+0.022}_{-0.030}$)
MINOS [10]	$0.041^{+0.047}_{-0.031}$ ($0.079^{+0.071}_{-0.053}$)	$0.010^{+0.012}_{-0.008}$ ($0.020^{+0.019}_{-0.014}$)
DC [11]	$0.086 \pm 0.041 \pm 0.030$	$0.022^{+0.019}_{-0.018}$
DYB [12]	$0.092 \pm 0.016 \pm 0.005$	0.024 ± 0.005
RENO [13]	$0.113 \pm 0.013 \pm 0.019$	0.029 ± 0.006

Table 2: The reactor angle measurements from the recent experiments T2K [9], MINOS [10], DOUBLE CHOOZ [11], Daya Bay [12] and RENO [13], for the normal (inverse) hierarchy.

angle, a relation known as quark-lepton complementarity [31–51]. Probably the exact complementarity relation becomes more plausible if replaced by $\theta_{12} + \mathcal{O}(\theta_C) \sim \pi/4$ (which we call “weak” complementarity). One can think of models where a suitable symmetry enforces BM mixing in the neutrino sector at leading order (LO) and the necessary, rather large, corrective terms to θ_{12} arise from the diagonalization of the charged lepton mass matrices [31–57]. Thus, if one or the other of these coincidences is taken seriously, models where TB or GR or BM mixing is naturally predicted are a good first approximation.

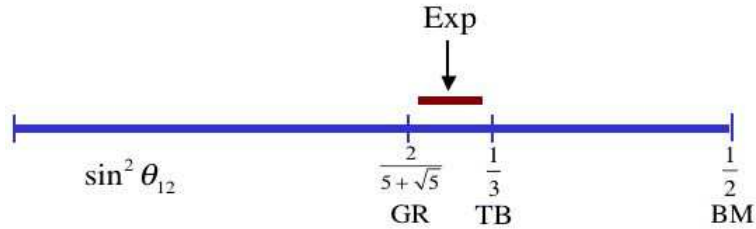


Figure 1: The values of $\sin^2 \theta_{12}$ for TB or GR or BM mixing are compared with the data at 1σ .

In the following we will mainly refer to TB or BM mixing which are the most studied first

approximations to the data. The simplest symmetry that, at LO, leads to TB is A_4 while BM can be obtained from S_4 . A_4 models have been studied widely (for a review and a list of references, see Ref. [14]). At LO the typical A_4 model leads to exact TB mixing. The LO approximation is then corrected by non-leading effects. Given the set of flavour symmetries and having specified the field content, the non-leading corrections to TB mixing, arising from higher dimensional effective operators, can be evaluated in a well-defined expansion. In the absence of specific dynamical tricks, in a generic model all three mixing angles receive corrections of the same order of magnitude. Since the experimentally allowed departures of θ_{12} from the TB value, $\sin^2 \theta_{12} = 1/3$, are small, numerically not larger than $\mathcal{O}(\lambda_C^2)$ where $\lambda_C = \sin \theta_C$, it follows that both θ_{13} and the deviation of θ_{23} from the maximal value are also expected to be typically of the same general size. The same qualitative conclusion also applies to A_5 models with GR mixing. This generic prediction of a small θ_{13} , numerically of $\mathcal{O}(\lambda_C^2)$, is now confronted with the most recent data. The central value $\sin \theta_{13} \sim 0.15$, from Table 1, is between $\mathcal{O}(\lambda_C^2) \sim \mathcal{O}(0.05)$ and $\mathcal{O}(\lambda_C) \sim \mathcal{O}(0.23)$. Since λ_C is not that small, this gap is not too large and one can argue that models based on TB (or GR) mixing are still viable with preference for the lower side of the experimental range.

Of course, one can introduce additional theoretical input to improve the value of θ_{13} (for an updated list of recent models of this kind see Ref. [58] and references therein; for recent models in the specific context of holographic composite Higgs see Refs. [59, 60]). In the case of A_4 , one particularly interesting example is provided by the Lin model [61] (see also Ref. [62]), formulated before the T2K, MINOS, DOUBLE CHOOZ, Daya Bay and RENO results. In the Lin model the A_4 symmetry breaking is arranged, by suitable additional Z_n parities, in a way that the corrections to the charged lepton and the neutrino sectors are kept separated not only at LO but also at next-to-leading order (NLO). This way, the contribution to neutrino mixing from the diagonalization of the charged leptons can be of $\mathcal{O}(\lambda_C^2)$, while those in the neutrino sector of $\mathcal{O}(\lambda_C)$. In addition, in the Lin model these large corrections do not affect θ_{12} and satisfy the relation $\sin^2 \theta_{23} = 1/2 + 1/\sqrt{2} \cos \delta \sin \theta_{13}$, with δ being the CKM-like CP violating phase of the lepton sector. Thus, in the Lin model the NLO corrections to the solar angle θ_{12} and to the reactor angle θ_{13} can be naturally of different orders.

Alternatively, one can think of models where, because of a suitable symmetry, BM mixing holds in the neutrino sector at LO and the corrective terms for θ_{12} , which in this case are necessarily rather large, arise from the diagonalization of charged lepton masses [31–57]. These terms from the charged lepton sector, numerically of order $\mathcal{O}(\lambda_C)$, would then generically also affect θ_{13} . The resulting value could well be compatible with the present experimental values of θ_{13} . An explicit model of this type based on the group S_4 has been developed in Ref. [52] (see also Refs. [53–55]). An important feature of this model is that only θ_{12} and θ_{13} are corrected by terms of $\mathcal{O}(\lambda_C)$ while θ_{23} is unchanged at this order. This model is compatible with present data and clearly prefers the upper range of the present experimental result for θ_{13} .

In this work we discuss three possible classes of models: 1) typical A_4 models where θ_{13} is generically expected to be small, of the order of the observed departures of θ_{12} from the TB value, and thus with preference for the lower end of the allowed experimental range. 2) special A_4 models, like the Lin model, where θ_{13} is disentangled from the deviation

of $\sin^2 \theta_{12}$ from the TB value $1/3$ and can be as large as the upper end of the allowed experimental range. We give a general characterization of these special A_4 models where the dominant corrections to TB mixing do not arise from the charged lepton sector but from the neutrino sector. 3) Models where BM mixing holds in the neutrino sector and large corrections to θ_{12} and θ_{13} arise from the diagonalization of charged leptons. The value of θ_{13} could naturally be close to the present experimental range. In each of these possible models the dominant corrections to the LO mixing pattern involve a number of parameters of the same order of magnitude, ξ . We discuss the success rate corresponding to the optimal value of ξ for each model, obtained by scanning the parameter space according to a similar procedure for all three cases. We argue that, while the absolute values of the success rates depend on the scanning assumptions, their relative values in the three classes of models, provide a reliable criterium for comparison. We find that, for reproducing the mixing angles, the Lin type models have the best performance, as expected, followed by the typical A_4 models while the BM mixing models lead to an inferior score, as they most often fail to reproduce θ_{12} .

We then discuss the implications for lepton flavour-violating (LFV) processes of the above three classes of possibilities, assuming a supersymmetric context, with or without See-Saw. The present bounds pose severe constraints on the parameter space of the models (for a recent general analysis on model-independent flavour violating effects in the context of flavour models, see Ref. [63]). In particular, we refer to the recent improved MEG result [64] on the $\mu \rightarrow e\gamma$ branching ratio, $Br(\mu \rightarrow e\gamma) \lesssim 2.4 \times 10^{-12}$ at 95% C.L. and to other similar processes like $\tau \rightarrow (e \text{ or } \mu)\gamma$. One expects that lepton flavour-violating processes may also have a large discriminating power in assessing the relative merits of the different models. We have studied this by adopting the simple CMSSM framework. While this overconstrained version of supersymmetry is rather marginal after the results of the LHC searches, more so if the Higgs mass really is around $m_H = 125$ GeV, we still believe it can be used here for our indicative purposes. We find that the most constrained versions are the models with BM mixing at LO where relatively large corrections directly appear in the off-diagonal terms of the charged lepton mass matrix. The A_4 models turn out to be the best suited to satisfy the experimental bounds, as the non-diagonal charged lepton matrix elements needed to reproduce the mixing angles are quite smaller. An intermediate score is achieved by the models of the Lin type, where the main corrections to the mixing angles arise from the neutrino sector. Overall the A_4 models emerge well from our analysis and in particular those of the Lin type perhaps appear as the most realistic approach to the data among the discrete flavour group models that we have studied. As for the regions of the CMSSM parameter space that are indicated by our analysis, the preference is for small $\tan \beta$ and large SUSY masses (at least one out of m_0 and $m_{1/2}$ must be above 1 TeV). As a consequence it appears impossible, at least within the CMSSM model, to satisfy the MEG bound and simultaneously reproduce the muon $g - 2$ discrepancy.

The paper is organized as follows. In Sect. 2 we discuss the models and their predictions for θ_{13} to then compare them with the data. In Sect. 3 we list the effective operators that induce lepton flavour violation and derive their contributions to the measured quantities. We then apply the general formalism to the specific models and observables. In Sect. 4 we derive our conclusions.

2 Models

We consider models invariant under a flavour symmetry group G_f . At the LO the lepton mixing arises from a mismatch between the residual symmetries G_e and G_ν of charged lepton and neutrino sectors, respectively. In this approximation charged leptons and neutrinos acquire mass from two independent sets of flavons, Φ_e and Φ_ν , whose VEVs preserve two Abelian groups: $G_e = Z_n$ ($n \geq 3$) and $G_\nu = Z_2 \times Z_2$. The groups G_e and G_ν can be subgroups of G_f or, as a result of the specific field content of the model and of the LO approximation, they can contain some accidental symmetry and generate a group G different from (and possibly larger than) G_f .¹ Lepton mass matrices can be expanded in inverse powers of the cut-off scale Λ

$$\begin{aligned} m_e &= m_e^{(0)} + \delta m_e^{(1)} + \dots \\ m_\nu &= m_\nu^{(0)} + \delta m_\nu^{(1)} + \dots \end{aligned} \quad (2.1)$$

where $\delta m_{e,\nu}^{(1)}/m_{e,\nu}^{(0)} = \mathcal{O}(\langle \Phi_{e,\nu} \rangle / \Lambda)$ and dots stand for higher-order terms. The LO contributions $m_e^{(0)}$ and $m_\nu^{(0)}$ depend only on $\langle \Phi_e \rangle$ and $\langle \Phi_\nu \rangle$, respectively. They are invariant under G_e and G_ν :

$$\begin{aligned} \rho(g_{ei})^\dagger m_e^{(0)\dagger} m_e^{(0)} \rho(g_{ei}) &= m_e^{(0)\dagger} m_e^{(0)}, \\ \rho(g_{\nu i})^T m_\nu^{(0)} \rho(g_{\nu i}) &= m_\nu^{(0)}. \end{aligned} \quad (2.2)$$

Here g_{ei} and $g_{\nu i}$ are the elements of G_e and G_ν and ρ denotes an irreducible three-dimensional unitary representation of the group G generated by G_e and G_ν .² Both G_e and G_ν are Abelian and the matrices $\rho(g_{ei})$ and $\rho(g_{\nu i})$ can be diagonalized by two independent unitary transformations Ω_e and Ω_ν

$$\rho(g_{\nu i})_{diag} = \Omega_\nu^\dagger \rho(g_{\nu i}) \Omega_\nu, \quad \rho(g_{ei})_{diag} = \Omega_e^\dagger \rho(g_{ei}) \Omega_e, \quad (2.3)$$

and the mixing matrix U_{PMNS} reflects the misalignment between the two bases:

$$U_{PMNS} = \Omega_e^\dagger \Omega_\nu. \quad (2.4)$$

It is immediate that the mixing matrix is independent of the choice of the basis. We choose to work in the basis where $\rho(g_{ei})$ and $m_e^{(0)\dagger} m_e^{(0)}$ are diagonal: $\Omega_e = 1$. Beyond LO, the prediction for the mixing in eq. (2.4) is modified. In general the VEVs of Φ_e and Φ_ν are corrected by terms of relative order $\langle \Phi_{e,\nu} \rangle / \Lambda$ and do not preserve G_e and G_ν any more. Moreover higher order operators contribute to lepton masses without respecting the LO residual symmetries. The NLO corrections are suppressed with respect to the LO contributions by the ratio between the flavon VEVs ($\langle \Phi_e \rangle, \langle \Phi_\nu \rangle$) and Λ . Depending on the agreement of the LO approximation to the data, $\langle \Phi_e \rangle / \Lambda$ and $\langle \Phi_\nu \rangle / \Lambda$ will typically range between λ_C^2 and λ_C .

¹ In the present paper we concentrate only on the TB, GR or BM patterns, originated by the mismatch between G_e and G_ν . However, interesting deformations of these patterns, all predicting already at the LO a non-vanishing θ_{13} , arise considering the finite modular groups Γ_N , $N > 1$: in Refs. [65,66], a comprehensive analysis is presented for an arbitrary G_e and $G_\nu = Z_2 \times Z_2$. In Refs. [67–69], a more general study has been presented, where the residual symmetry in the neutrino sector is $G_\nu = Z_2$, while the other Z_2 component arises accidentally.

² Later on we will include in $m_e^{(0)}$ also higher-order contributions satisfying the property (2.2).

2.1 A_4 Models

We refer to SUSY models based on the flavour symmetry $G_f = A_4 \times G_{AUX}$, where the G_{AUX} factor depends on the specific realization [61, 70–72].³ The group A_4 can be generated by two elements S and T satisfying

$$S^2 = (ST)^3 = T^3 = 1. \quad (2.5)$$

The irreducible representations of A_4 are a triplet 3 and three inequivalent singlets 1, 1' and 1''. In the triplet representation S and T can be chosen as:

$$T = \begin{pmatrix} 1 & 0 & 0 \\ 0 & \omega^2 & 0 \\ 0 & 0 & \omega \end{pmatrix}, \quad S = \frac{1}{3} \begin{pmatrix} -1 & 2 & 2 \\ 2 & -1 & 2 \\ 2 & 2 & -1 \end{pmatrix}, \quad (2.6)$$

where $\omega = e^{i2\pi/3}$. Under A_4 the electroweak SU(2) lepton doublets l transform as a triplet, while the electroweak singlets e^c , μ^c and τ^c and the electroweak Higgs doublets $H_{u,d}$ as singlets. In the flavon sector both Φ_e and Φ_ν always include a triplet, but they can also include additional singlets. At the LO and in the exact SUSY limit the VEVs of Φ_e and Φ_ν are determined by two separate sets of equations and satisfy at LO:

$$T' \langle \Phi_e \rangle = \langle \Phi_e \rangle, \quad S \langle \Phi_\nu \rangle = \langle \Phi_\nu \rangle. \quad (2.7)$$

The transformation T' can coincide with the T generator of A_4 [70, 71], or can represent an accidental symmetry of the charged lepton Lagrangian still satisfying $T'^3 = 1$, as in the models of Refs. [61, 72], where $T' = \omega T$. The charged lepton mass matrix m_e is given by

$$m_e = m_e^{(0)} + \delta m_e^{(1)} + \dots \quad (2.8)$$

where

$$m_e^{(0)} = v_d \begin{pmatrix} y_e & 0 & 0 \\ 0 & y_\mu & 0 \\ 0 & 0 & y_\tau \end{pmatrix} \eta. \quad (2.9)$$

Here v_d is the VEV of H_d , y_f ($f = e, \mu, \tau$) are dimensionless quantities and η is a small parameter that breaks the flavour symmetry A_4 . At the LO the charged lepton mass matrix $m_e^{(0)}$, only depending on $\langle \Phi_e \rangle$, is diagonal and invariant under the action of the transformation T' :

$$T'^\dagger m_e^{(0)\dagger} m_e^{(0)} T' = m_e^{(0)\dagger} m_e^{(0)}. \quad (2.10)$$

We have $G_e = Z_3$, generated by T' . The hierarchical pattern $y_e \ll y_\mu \ll y_\tau$ can be reproduced by requiring that operators of increasing dimension contribute to y_τ , y_μ and y_e ,

³The present analysis applies also to models based on flavour symmetries that contain the group A_4 , such as S_4 : few examples can be found in Refs. [73–76], where the TB pattern is predicted at the LO, while at the NLO the mixing is corrected in a similar way as we are going to discuss in this section. Moreover, our analysis applies also to the model based on the flavour group T' , described in Ref. [77], even if T' does not contain A_4 as a subgroup. Although we could generalize our analysis to a broader class of symmetries, we focus on the flavour group A_4 that represents the minimal choice in terms of dimensions of a group.

respectively ⁴. This can be achieved either by means of a Froggatt-Nielsen $U(1)$ symmetry contained in G_{AUX} [70,71] or through some discrete components of G_{AUX} as in Refs. [61,72].

This class of models can be realized both with and without a See-Saw mechanism. In the first case there are three right-handed neutrinos transforming as a triplet of A_4 , while in the second case the source of neutrino masses is a set of higher dimensional operators violating the total lepton number. In either case the light neutrino mass matrix m_ν is given by:

$$m_\nu = m_\nu^{(0)} + \delta m_\nu^{(1)} + \dots \quad (2.11)$$

where

$$m_\nu^{(0)} = \begin{pmatrix} x & y & y \\ y & x+z & y-z \\ y & y-z & x+z \end{pmatrix}. \quad (2.12)$$

The parameters x , y and z are quadratic in v_u , the VEV of H_u , and inversely proportional to the scale associated with the violation of the total lepton number. The LO term $m_\nu^{(0)}$ is invariant under the $Z_2 \times Z_2$ symmetry generated by S , eq. (2.7), and by

$$A_{23} = \begin{pmatrix} 1 & 0 & 0 \\ 0 & 0 & 1 \\ 0 & 1 & 0 \end{pmatrix}. \quad (2.13)$$

Indeed,

$$S^T m_\nu^{(0)} S = m_\nu^{(0)} \quad \text{and} \quad A_{23}^T m_\nu^{(0)} A_{23} = m_\nu^{(0)}. \quad (2.14)$$

The Z_2 symmetry generated by the matrix A_{23} is an accidental symmetry. The matrix $m_\nu^{(0)}$ of eq. (2.12) is the most general one invariant under both S and A_{23} . In the minimal formulation of Refs. [61,70,71] the parameters x , y and z are not independent. If neutrino masses are generated via the See-Saw mechanism [61,71] they are related by

$$z = \frac{(x-y)^2}{4y-x}. \quad (2.15)$$

If neutrino masses are parametrized directly through a higher dimensional operator [70,71] we have

$$z = -(x+2y). \quad (2.16)$$

At the LO $m_e^{(0)}$ is diagonal while $m_\nu^{(0)}$ is diagonalized by

$$U_{TB} = \begin{pmatrix} \sqrt{\frac{2}{3}} & \sqrt{\frac{1}{3}} & 0 \\ -\sqrt{\frac{1}{6}} & \sqrt{\frac{1}{3}} & -\sqrt{\frac{1}{2}} \\ -\sqrt{\frac{1}{6}} & \sqrt{\frac{1}{3}} & \sqrt{\frac{1}{2}} \end{pmatrix}. \quad (2.17)$$

This holds for any value of the parameters x , y and z since U_{TB} simultaneously diagonalizes both S and A_{23} .

⁴Here, we include in $m_e^{(0)}$ all contributions arising from the LO $\langle \Phi_e \rangle$, independently of the dimensionality of the corresponding operator.

The departure from the LO approximation depends on the subleading contributions $\delta m_e^{(1)}$ and $\delta m_\nu^{(1)}$, which can vary for different models. In all models considered here [61, 70–72] the NLO correction to the charged lepton mass matrix is not invariant under T' and is of the following type:

$$\delta m_e^{(1)} = v_d \begin{pmatrix} \mathcal{O}(y_e) & \mathcal{O}(y_e) & \mathcal{O}(y_e) \\ \mathcal{O}(y_\mu) & \mathcal{O}(y_\mu) & \mathcal{O}(y_\mu) \\ \mathcal{O}(y_\tau) & \mathcal{O}(y_\tau) & \mathcal{O}(y_\tau) \end{pmatrix} \eta \xi, \quad (2.18)$$

where ξ is a small adimensional parameter given by the ratio between a flavon VEVs and Λ . The transformation to diagonalize m_e is $V_e^T m_e U_e = m_e^{diag}$ with

$$U_e = \begin{pmatrix} 1 & c_{12}^e \xi & c_{13}^e \xi \\ -c_{12}^{e*} \xi & 1 & c_{23}^e \xi \\ -c_{13}^{e*} \xi & -c_{23}^{e*} \xi & 1 \end{pmatrix} \quad (2.19)$$

where c_{12}^e , c_{13}^e and c_{23}^e are complex parameters of order one in absolute value. We discuss the NLO contribution to m_ν by distinguishing two cases.

2.1.1 Typical A_4 Models

In “typical” A_4 models [71, 72], the NLO contribution $\delta m_\nu^{(1)}$ is a generic symmetric matrix with entries suppressed, compared to the corresponding entries in $m_\nu^{(0)}$, by a relative factor ξ' , of the order of the ratio between a flavon VEV and Λ . This occurs both with and without the See-Saw mechanism. The generic transformation that diagonalize m_ν is $U_{TB} \cdot U_\nu$ where

$$U_\nu = \begin{pmatrix} 1 & c_{12}^{\nu'} \xi' & c_{13}^{\nu'} \xi' \\ -c_{12}^{\nu'*} \xi' & 1 & c_{23}^{\nu'} \xi' \\ -c_{13}^{\nu'*} \xi' & -c_{23}^{\nu'*} \xi' & 1 \end{pmatrix}, \quad (2.20)$$

where $c_{12}^{\nu'}$, $c_{13}^{\nu'}$ and $c_{23}^{\nu'}$ are complex parameters of order one in absolute value. Barring a fine tuning of the Lagrangian parameters, in these models the suppression factors ξ and ξ' are expected to be of the same order of magnitude. For example, beyond the LO the equations satisfied by $\langle \Phi_e \rangle$ and $\langle \Phi_\nu \rangle$ are no longer decoupled and the corrections to the LO flavon VEVs are of the same size, for both Φ_e and Φ_ν . All the elements of the mixing matrix get corrections of the same size $\xi \approx \xi'$. We expect⁵:

$$\begin{aligned} \sin^2 \theta_{23} &= \frac{1}{2} + \mathcal{R}e(c_{23}^e) \xi + \frac{1}{\sqrt{3}} \left(\mathcal{R}e(c_{13}^{\nu'}) - \sqrt{2} \mathcal{R}e(c_{23}^{\nu'}) \right) \xi \\ \sin^2 \theta_{12} &= \frac{1}{3} - \frac{2}{3} \mathcal{R}e(c_{12}^e + c_{13}^e) \xi + \frac{2\sqrt{2}}{3} \mathcal{R}e(c_{12}^{\nu'}) \xi \\ \sin \theta_{13} &= \frac{1}{6} \left| 3\sqrt{2}(c_{12}^e - c_{13}^e) + 2\sqrt{3} \left(\sqrt{2} c_{13}^{\nu'} + c_{23}^{\nu'} \right) \right| \xi. \end{aligned} \quad (2.22)$$

⁵Eq. (2.22) is a particular case of the general parametrization presented Ref. [78]:

$$\sin \theta_{23} = \frac{1}{\sqrt{2}}(1 + a), \quad \sin \theta_{12} = \frac{1}{\sqrt{3}}(1 + s), \quad \sin \theta_{13} = \frac{r}{\sqrt{2}}, \quad (2.21)$$

with a , s and r real numbers. The expressions in Eq. (2.22) show explicitly the dependence of the NLO mixing angles on the corrections from both the neutrino and the charged lepton sectors.

We see that to reach the central value for the reactor angle in agreement with the value reported in Table 1, the parameter ξ should be of $\mathcal{O}(0.1)$. A precise value can be found studying the success rate to reproduce all the three mixing angles inside the corresponding 3σ ranges, depending on the value of ξ . As shown in Fig. 2, the value of ξ that maximizes the success rate is 0.076(0.077) for NH (IH). The corresponding value is $\sim 8.5\%$, which is not large but not hopelessly small either.

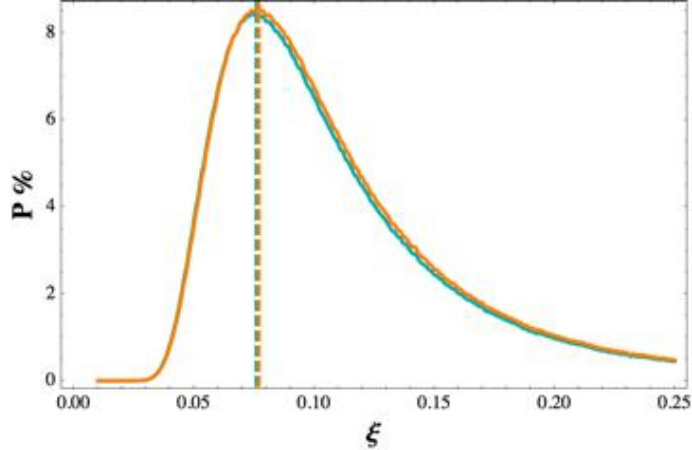


Figure 2: **Typical A_4 Models.** Success Rates as a function of the parameter ξ . The $c_{ij}^{e,\nu}$ parameters that multiply ξ are treated as random complex numbers with absolute values following a Gaussian distribution around 1 with variance 0.5. In Cyan the NH and in Orange the IH. The value of ξ that maximizes the success rate is 0.076(0.077) for NH (IH).

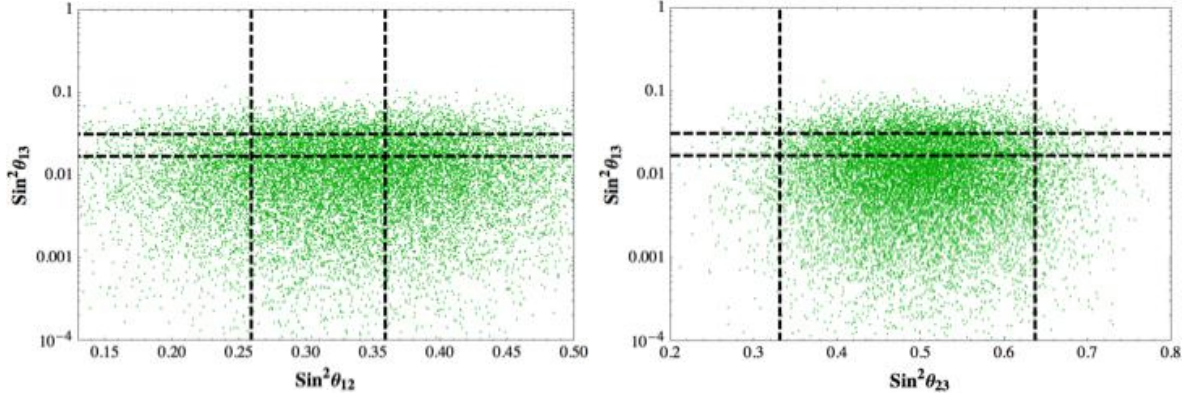
We analyze quantitatively the expressions in eq. (2.22) and their correlations in Fig. 3: in the plots on the left (right), we show the correlation between $\sin^2 \theta_{13}$ and $\sin^2 \theta_{12}$ ($\sin^2 \theta_{23}$). The parameter ξ is taken equal to 0.076. The $c_{ij}^{e,\nu}$ parameters that multiply ξ are treated as random complex numbers with absolute values following a Gaussian distribution around 1 with variance 0.5. In the plots we show only the NH case. The IH case is similar.

As we can see, the plots are representing the general behaviour of this class of models: $\sin^2 \theta_{13}$ increases with ξ , but correspondingly also the deviation of $\sin^2 \theta_{12}$ from $1/3$ does. As a result, even for the value of ξ that maximizes the success rate, the requirement for having a reactor angle inside its 3σ error range corresponds to a prediction for the solar angle that spans all the 3σ experimental error bar and is often not even in agreement with the data.

2.1.2 Special A_4 Models

In these models the accidental symmetry A_{23} of the neutrino sector is broken by a relatively large amount so that, in first approximation, the residual symmetries of the charged lepton and neutrino sectors are those generated by T' and S , respectively. At the LO and in the chosen basis $m_e^\dagger m_e$ is diagonal while m_ν is invariant under S :

$$S^T m_\nu S = m_\nu. \quad (2.23)$$



(a) Correlation between $\sin^2 \theta_{12}$ and $\sin^2 \theta_{13}$.

(b) Correlation between $\sin^2 \theta_{23}$ and $\sin^2 \theta_{13}$.

Figure 3: **Typical A_4 Models.** On the left (right), we plot $\sin^2 \theta_{13}$ as a function of $\sin^2 \theta_{12}$ ($\sin^2 \theta_{23}$), following eq. (2.22). The dashed-black lines represent the 3σ values for the mixing angles from the Fogli *et al.* fit [7]. Only the NH data sets is shown. The parameter ξ is taken equal to 0.076. The $c_{ij}^{\epsilon,\nu}$ parameters that multiply ξ are treated as random complex numbers with absolute values following a Gaussian distribution around 1 with variance 0.5.

The most general solution to this constraint can be parametrized in the following form:

$$m_\nu = \begin{pmatrix} x & y - w & y + w \\ y - w & x + z + w & y - z \\ y + w & y - z & x + z - w \end{pmatrix}, \quad (2.24)$$

We see that w describes the deviation of m_ν from the form associated to the Tri-Bimaximal mixing, see eq. (2.12). The matrix m_ν can be diagonalized in two steps. First we transform m_ν by a Tri-Bimaximal rotation:

$$m'_\nu = U_{TB}^T m_\nu U_{TB} = \begin{pmatrix} x - y & 0 & \sqrt{3}w \\ 0 & x + 2y & 0 \\ \sqrt{3}w & 0 & x - y + 2z \end{pmatrix}. \quad (2.25)$$

Second, we perform a unitary transformation in the (1,3) plane:

$$V = \begin{pmatrix} \alpha & 0 & \xi' \\ 0 & 1 & 0 \\ -\xi'^* & 0 & \alpha^* \end{pmatrix}, \quad |\alpha|^2 + |\xi'|^2 = 1, \quad (2.26)$$

$$V^T m'_\nu V = m_\nu^{diag}. \quad (2.27)$$

The exact rotation is given by:

$$\frac{2\alpha\xi'}{|\alpha|^2 - |\xi'|^2} = \frac{uv^*(u^* - v)}{|v|^2 - |u|^2}, \quad \text{with} \quad u \equiv \frac{2\sqrt{3}w}{x - y}, \quad \text{and} \quad v \equiv -\frac{2\sqrt{3}w}{x - y + 2z}. \quad (2.28)$$

The unitary matrix that diagonalizes m_ν is

$$U_{TB}V = \begin{pmatrix} \sqrt{2/3}\alpha & 1/\sqrt{3} & \sqrt{2/3}\xi' \\ -\alpha/\sqrt{6} + \xi'^*/\sqrt{2} & 1/\sqrt{3} & -\alpha^*/\sqrt{2} - \xi'/\sqrt{6} \\ -\alpha/\sqrt{6} - \xi'^*/\sqrt{2} & 1/\sqrt{3} & +\alpha^*/\sqrt{2} - \xi'/\sqrt{6} \end{pmatrix}. \quad (2.29)$$

Such a mixing pattern is very interesting because the observed θ_{13} can be reproduced by choosing ξ' of order 0.1 and the predicted value of $\sin^2 \theta_{12}$ deviates from $1/3$ only by terms of order ξ'^2 . To preserve these properties corrections from the charged lepton sector should be small compared to ξ' . This can be realized by adopting two different expansion parameters $\xi \ll \xi'$ for the charged lepton sector and for the neutrino sector. A model along these lines has been built in Ref. [61]. The setup is arranged in such a way that $\langle \Phi_e \rangle$ and $\langle \Phi_\nu \rangle$ satisfy decoupled equations up to NLO so that it is possible to achieve $\langle \Phi_e \rangle \ll \langle \Phi_\nu \rangle$ and to maintain the property of eq. (2.7) up to NLO. Moreover $\langle \Phi_\nu \rangle$ couples to charged leptons only at the NNLO so that the dominant source of corrections to the neutrino mixing pattern is $\delta m_\nu^{(1)}$, which in turns, being dominated by $\langle \Phi_\nu \rangle$, is invariant under S .

In eq. (2.29) it is not restrictive to choose α real and positive and we have:

$$\delta_{CP} \approx \arg \xi' \quad (2.30)$$

$$\sin \theta_{13} = \left| \sqrt{\frac{2}{3}} \xi' + \frac{c_{12}^e - c_{13}^e}{\sqrt{2}} \xi \right| \quad (2.31)$$

$$\begin{aligned} \sin^2 \theta_{12} &= \frac{1}{3 - 2|\xi'|^2} - \frac{2}{3} \mathcal{R}e(c_{12}^e + c_{13}^e) \xi \\ &= \frac{1}{3} + \frac{2}{9} |\xi'|^2 - \frac{2}{3} \mathcal{R}e(c_{12}^e + c_{13}^e) \xi \end{aligned} \quad (2.32)$$

$$\begin{aligned} \sin^2 \theta_{23} &= \frac{1}{2} \frac{\left(1 + \frac{\xi'}{\sqrt{3}\alpha}\right) \left(1 + \frac{\xi'^*}{\sqrt{3}\alpha}\right)}{\left(1 + \frac{|\xi'|^2}{3\alpha^2}\right)} + \mathcal{R}e(c_{23}^e) \xi \\ &= \frac{1}{2} + \frac{1}{\sqrt{3}} |\xi'| \cos \delta_{CP} + \mathcal{R}e(c_{23}^e) \xi \end{aligned} \quad (2.33)$$

where we have also included the effects coming from the diagonalization of the charged lepton sector as in eq. (2.19), to first order in ξ . The second equality shows the result expanded in powers of $|\xi'|$, to the order $|\xi'|^2$. In these models $|\xi'|$ is chosen to be of order 0.1, larger than ξ so that the contribution of eq. (2.19) can be neglected, and the lepton mixing matrix is very close to $U_{TB}V$. It is interesting to note that if we neglect the corrections proportional to ξ , we have exact correlations between the reactor angle and the other two angles⁶:

$$\sin^2 \theta_{12} = \frac{1}{3(1 - \sin^2 \theta_{13})}, \quad \sin^2 \theta_{23} = \frac{1}{2} + \frac{1}{\sqrt{2}} \sin \theta_{13} \cos \delta_{CP}. \quad (2.34)$$

⁶It has been shown in Ref. [69], from general group theoretical considerations, that these correlations are a general feature of flavour models when the symmetry group of the charged lepton (neutrino) mass matrix is Z_3 (Z_2).

The first expression shows that the unitary transformation V always increases the solar angle from the TB value, while the preferred 1σ interval is below the TB prediction, see Fig. 1. This is a small effect, of second order in θ_{13} , that can be compensated by the corrections proportional to ξ . The second correlation involves the Dirac CP phase and is particularly interesting considering the recent hint of a CP phase close to π for the NH case. In Fig. 4, we graphically compare this second expression with the present data for the NH case: when considering the 1σ (2σ) ranges for the mixing angles, one sees an indication that $\cos\delta_{CP}$ lies in the interval $[-1, -0.5]$, while no indication arises when the 3σ error band for $\sin^2\theta_{23}$ is taken into account. Although these results for the CP phase is modified by the inclusion of the subleading ξ contributions, these correlations will allow an interesting test for such models once δ_{CP} is measured and the precision on $\sin^2\theta_{23}$ is improved.

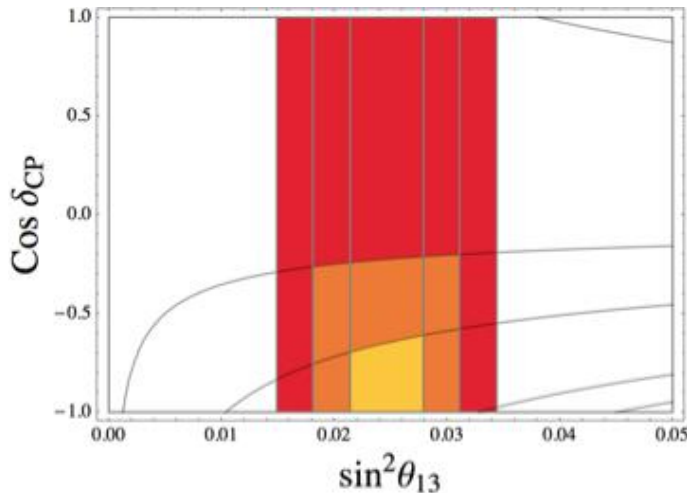


Figure 4: **Special A_4 Models.** Contour plot for 1, 2, 3σ values of $\sin^2\theta_{23}$ in the parameter space $\sin^2\theta_{13}-\cos\delta_{CP}$ according to the values for the NH in Table 1. The Yellow, Orange, Red regions refer to the data at 1σ , 2σ , 3σ , respectively.

In Fig. 5, we study the success rate to reproduce all the three mixing angles inside their corresponding 3σ error ranges, as a function of $|\xi'|$. The parameters have been chosen such that ξ is a real number in $[0.005, 0.06]$ and c_{ij}^e are random complex numbers with absolute values following a Gaussian distribution around 1 with variance 0.5. The value of $|\xi'|$ that maximizes the success rate for both NH and IH is 0.184. The corresponding success rate is much larger in these models ($\sim 55\%$) than for the typical A_4 models.

We analyze quantitatively the deviations in eqs. (2.32) and (2.33) and their correlations in Fig. 6: in the plots on the left (right) column, we show the correlations in eqs. (2.32) and (2.33) between $\sin^2\theta_{13}$ and $\sin^2\theta_{12}$ or $\sin^2\theta_{23}$, respectively. The parameters have been chosen such that ξ is a real number in $[0.005, 0.06]$; ξ' is a complex number with absolute values equal to 0.184; the parameters c_{ij}^e are random complex numbers with absolute values following a Gaussian distribution around 1 with variance 0.5. In the plots we show only the NH case. The IH case is similar. For this choice of the parameters, the model can well describe all three angles inside the corresponding 3σ interval, and its success rate is much

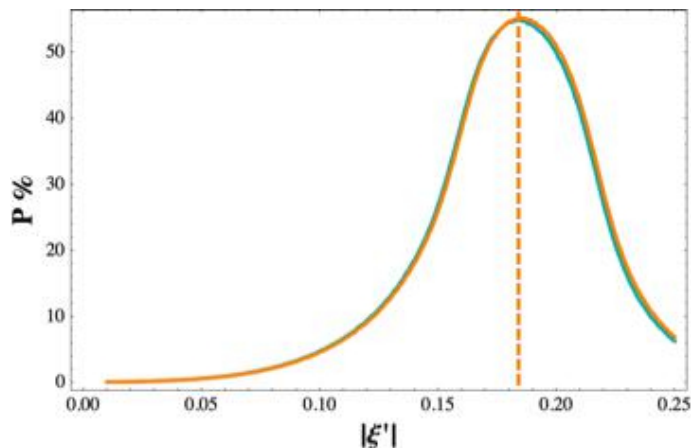
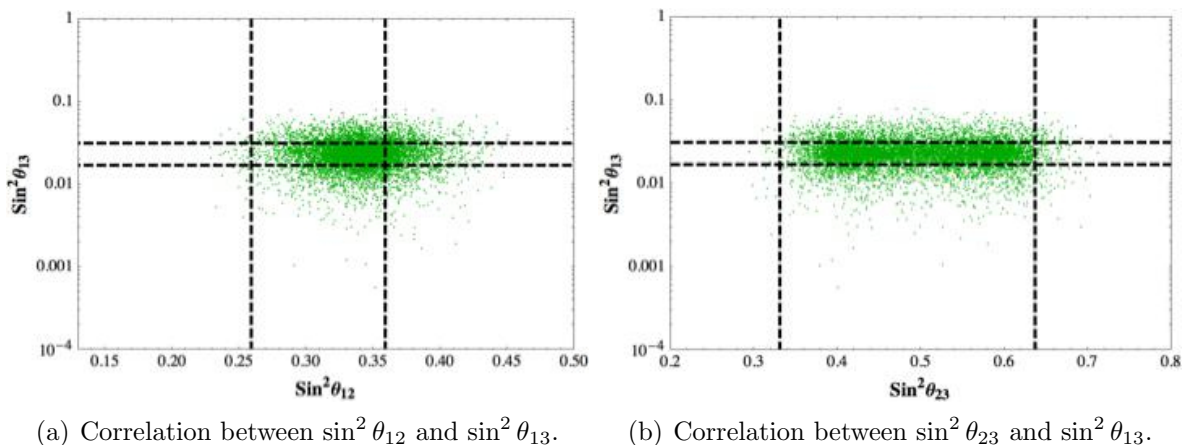


Figure 5: **Special A_4 Models.** Success Rates as a function of the parameter $|\xi'|$. The parameters have been chosen such that ξ is a real number in $[0.005, 0.06]$ and c_{ij}^e are random complex numbers with absolute values following a Gaussian distribution around 1 with variance 0.5. In Cyan the NH and in Orange the IH. The value of $|\xi'|$ that maximizes the success rate for both NH and IH is 0.184.

larger than that of the typical TB models, as turns out by comparing Figs. 2 and 5.



(a) Correlation between $\sin^2 \theta_{12}$ and $\sin^2 \theta_{13}$.

(b) Correlation between $\sin^2 \theta_{23}$ and $\sin^2 \theta_{13}$.

Figure 6: **Special A_4 Models.** $\sin^2 \theta_{13}$ as a function of $\sin^2 \theta_{12}$ ($\sin^2 \theta_{23}$) is plotted on the left (right), following eqs. (2.32) and (2.33). The dashed-black lines represent the 3σ values for the mixing angles from the Fogli *et al.* fit [7]. Only the NH data sets is shown. The parameter ξ is a real number in $[0.005, 0.06]$; ξ' is a complex number with absolute values equal to 0.184; the parameters c_{ij}^e are random complex numbers with absolute values following a Gaussian distribution around 1 with variance 0.5.

2.2 S_4 Models

In this section we refer to a SUSY model based on the flavour symmetry $G_f = S_4 \times Z_4 \times U(1)$ [52], but we keep the presentation slightly more general, to embrace a wider

class of possibilities [53–55]. The group S_4 admits two generators S and T satisfying

$$S^2 = (ST)^3 = T^4 = 1. \quad (2.35)$$

Its irreducible representations are two singlets 1 and $1'$, a doublet 2 and two triplets 3 and $3'$. In one of the two triplet representations of S_4 , S and T can be chosen as:

$$T = \begin{pmatrix} -1 & 0 & 0 \\ 0 & -i & 0 \\ 0 & 0 & i \end{pmatrix}, \quad S = \begin{pmatrix} 0 & -\frac{1}{\sqrt{2}} & -\frac{1}{\sqrt{2}} \\ -\frac{1}{\sqrt{2}} & \frac{1}{2} & -\frac{1}{2} \\ -\frac{1}{\sqrt{2}} & -\frac{1}{2} & \frac{1}{2} \end{pmatrix}. \quad (2.36)$$

In the class of models considered here the electroweak $SU(2)$ lepton doublets l transform as a triplet 3, the electroweak singlets e^c , μ^c and τ^c transform as singlets and the electroweak Higgs doublets $H_{u,d}$ are invariant. If present, the right-handed neutrinos transform as a triplet 3. Similarly to the previous class of models, at the LO and in the SUSY limit the VEVs of Φ_e and Φ_ν are determined by two decoupled equations and satisfy

$$T'\langle\Phi_e\rangle = \langle\Phi_e\rangle, \quad S\langle\Phi_\nu\rangle = \langle\Phi_\nu\rangle \quad [\text{LO}]. \quad (2.37)$$

The transformation $T' = iT$ generates a Z_4 subgroup of the flavour group G_f [52]. The charged lepton mass matrix m_e is given by

$$m_e = m_e^{(0)} + \delta m_e^{(1)} + \dots \quad (2.38)$$

with the LO contribution $m_e^{(0)}$ of the same type as the one considered before in eq. (2.9). In this case, η represents a small parameter that breaks the flavour symmetry S_4 . At the LO the charged lepton mass matrix $m_e^{(0)}$, only depending on $\langle\Phi_e\rangle$, is diagonal and invariant under the action of the transformation T' :

$$T'^\dagger m_e^{(0)\dagger} m_e^{(0)} T' = m_e^{(0)\dagger} m_e^{(0)}. \quad (2.39)$$

We have $G_e = Z_4$, generated by T' . The hierarchical pattern $y_e \ll y_\mu \ll y_\tau$ is reproduced by operators of increasing dimensions contributing to y_τ , y_μ and y_e , respectively. Also in this case we are including in $m_e^{(0)}$ all terms arising from the LO $\langle\Phi_e\rangle$, independently from the dimensionality of the operators that contribute to the charged lepton mass matrix.

In the specific model of Ref. [52] a See-Saw mechanism produces a mass matrix for the light neutrinos m_ν , given by:

$$m_\nu = m_\nu^{(0)} + \delta m_\nu^{(1)} + \dots \quad (2.40)$$

where

$$m_\nu^{(0)} = \begin{pmatrix} x & y & y \\ y & z & x - z \\ y & x - z & z \end{pmatrix}.$$

The parameters x , y and z are quadratic in v_u , the VEV of H_u and inversely proportional to the scale associated with the violation of the total lepton number. The LO term $m_\nu^{(0)}$ is

invariant under the $Z_2 \times Z_2$ symmetry generated by S , eq. (2.37), and by the transformation A_{23} of eq. (2.13):

$$S^T m_\nu^{(0)} S = m_\nu^{(0)}, \quad A_{23}^T m_\nu^{(0)} A_{23} = m_\nu^{(0)}. \quad (2.41)$$

Also in this case the Z_2 symmetry represented by the matrix A_{23} is an accidental symmetry. The matrix $m_\nu^{(0)}$ of eq. (2.41) is the most general one invariant under both S and A_{23} . In the realization of Ref. [52] the parameters x , y and z are related by

$$z = x - \frac{y^2}{x}. \quad (2.42)$$

At the LO $m_e^{(0)}$ is diagonal while $m_\nu^{(0)}$ is diagonalized by

$$U_{BM} = \begin{pmatrix} \sqrt{\frac{1}{2}} & -\sqrt{\frac{1}{2}} & 0 \\ \frac{1}{2} & \frac{1}{2} & -\sqrt{\frac{1}{2}} \\ \frac{1}{2} & \frac{1}{2} & \sqrt{\frac{1}{2}} \end{pmatrix}. \quad (2.43)$$

This holds for any value of the parameters x , y and z since U_{BM} is the matrix that simultaneously diagonalizes S and A_{23} .

The departure from the bimaximal mixing depends on the subleading contributions $\delta m_e^{(1)}$, $\delta m_\nu^{(1)}$. In the model of Ref. [52], such contributions are not generic. At the NLO the corrections to both the neutrino and the charged lepton sector are controlled by $\langle \Phi_\nu \rangle$ which preserves the LO alignment. The NLO correction to the charged lepton mass matrix is no longer invariant under T' and is of the following type:

$$\delta m_e^{(1)} = v_d \begin{pmatrix} \mathcal{O}(y_e) & \mathcal{O}(y_e) & \mathcal{O}(y_e) \\ \mathcal{O}(y_\mu) & \mathcal{O}(y_\mu) & 0 \\ \mathcal{O}(y_\tau) & 0 & \mathcal{O}(y_\tau) \end{pmatrix} \eta \xi,$$

where ξ is a small adimensional parameter given by the ratio between a flavon of the Φ_ν sector and Λ . The transformation needed to diagonalize m_e is $V_e^T m_e U_e = m_e^{diag}$ where, to first order in ξ

$$U_e = \begin{pmatrix} 1 & c_{12}^e \xi & c_{13}^e \xi \\ -c_{12}^{e*} \xi & 1 & 0 \\ -c_{13}^{e*} \xi & 0 & 1 \end{pmatrix}, \quad (2.44)$$

where c_{ij}^e are complex number with absolute value of order one. In the neutrino sector after the inclusion of the NLO corrections the mass matrix has still the form of eq. (2.41) and is diagonalized by U_{BM} . The lepton mixing is $U_e^\dagger U_{BM}$ and to first order in ξ we have

$$\begin{aligned} \delta_{CP} &= \pi + \arg(c_{12}^e - c_{13}^e) \\ \sin \theta_{13} &= \frac{1}{\sqrt{2}} |c_{12}^e - c_{13}^e| \xi \\ \sin^2 \theta_{12} &= \frac{1}{2} - \frac{1}{\sqrt{2}} \mathcal{R}e(c_{12}^e + c_{13}^e) \xi \\ \sin^2 \theta_{23} &= \frac{1}{2}. \end{aligned} \quad (2.45)$$

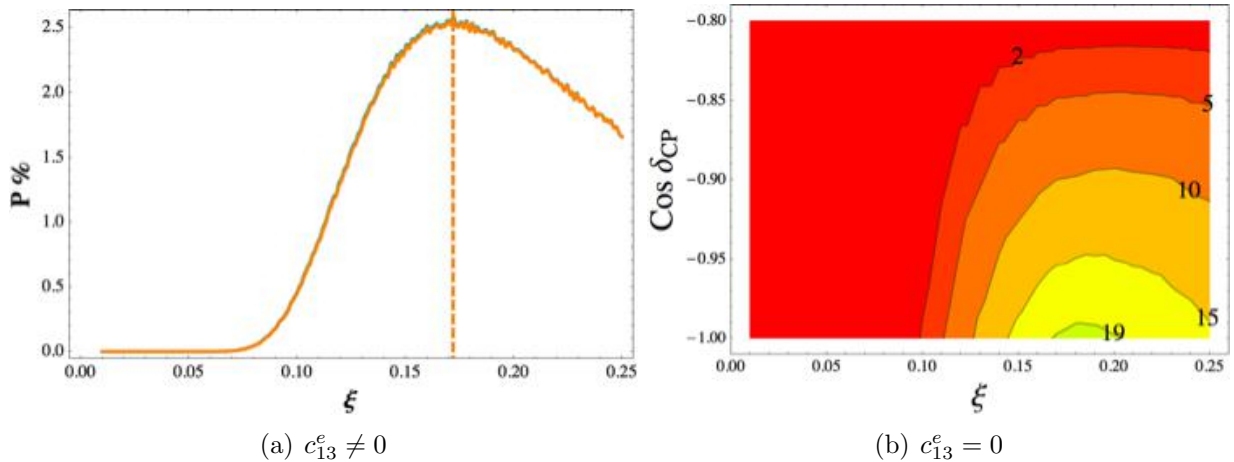


Figure 7: **S_4 Models.** In (a), the success rate as a function of the parameter ξ . The parameters $c_{12,13}^e$ have been taken as random complex numbers with absolute value following a Gaussian distribution around 1 with variance 0.5. In Cyan the NH and in Orange the IH. The value of ξ that maximizes the success rate shown in the left plot is $\xi = 0.172$, for both the NH and IH. In (b), the success rate for the case $c_{13}^e = 0$ as a function of ξ and $\cos \delta_{CP}$. The parameters c_{12}^e is been taken as a random complex number with absolute value following a Gaussian distribution around 1 with variance 0.5. The success rate reaches its maximum, $\sim 20\%$, for $\cos \delta_{CP} = -1$ and $\xi = 0.18$. Only the NH case is shown. The IH is similar.

To properly correct the BM value of the solar angle to agree with the data, ξ is expected to be $\mathcal{O}(\lambda_C)$. Studying the success rate of having all three mixing angles inside the corresponding 3σ ranges, we find that it is maximized for both the NH and IH when $\xi = 0.172$, as shown in Fig. 7(a). In this case, the maximal success rate of about 2.6% is particularly small. The problem for this model is not to reproduce θ_{13} but rather to calibrate the correction to θ_{12} for it to fall in its allowed window: we see from Fig. 7(a) that most of the scanning points spread out in a large interval of $\sin^2 \theta_{12}$ between ~ 0.2 and ~ 0.8 . It may be interesting in this case to explore the possibility that one of the charged lepton mixing angles is dominant. For this to occur naturally an additional dynamical input would be needed. For the specific case $c_{13}^e = 0$, we get a even more predictive correlation (still dependent, through δ_{CP} , on the c_{12}^e phase) among the solar and the reactor angle:

$$\sin^2 \theta_{12} = \frac{1}{2} + \sin \theta_{13} \cos \delta_{CP} + \mathcal{O}(\sin^2 \theta_{13}). \quad (2.46)$$

In this case, we study the dependence of the success rate from both ξ and the Dirac CP phase, in terms of $\cos \delta_{CP}$: being dependent on two parameters, this success rate cannot be directly compared with the previous one, function of only ξ ; a trustworthy comparison requires to average among all the values of the success rate for a fixed ξ . The corresponding plot for the NH case is shown in Fig. 7(b): the success rate reaches its maximum, $\sim 20\%$, for $\xi = 0.18$ and $\cos \delta_{CP} = -1$, for both the NH and IH cases. Only the NH case is shown in Fig. 7(b), while the IH is similar. The alternative possibility that $c_{12}^e = 0$ would lead to

similar results.

It is interesting to investigate the origin of the preference for $\delta_{CP} = -1$ shown in Fig. 7(b). In Fig. 8, we graphically present the correlation in Eq. (2.46), neglecting the $\mathcal{O}(\sin^2\theta_{13})$ terms. The predicted value of $\sin^2\theta_{12}$ agrees with the experimental one only when $\cos\delta_{CP}$ is very close to -1 . Although this correlation is modified once subleading contributions from both the neutrino and the charged lepton sectors are taken into account, still it will provide a strong test for such models.

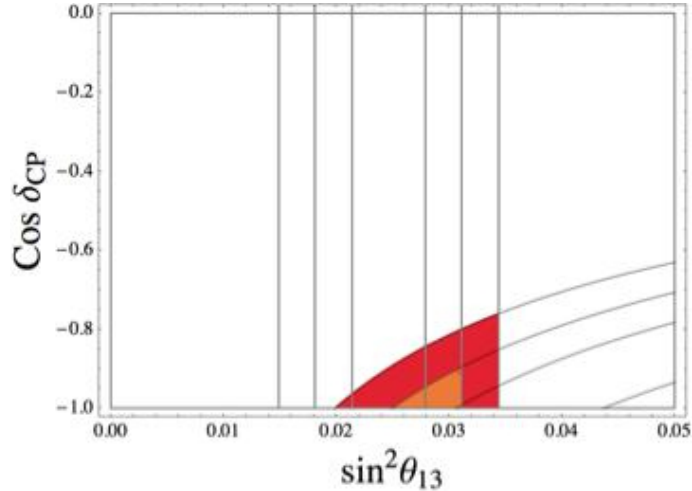


Figure 8: **S_4 Models.** Contour plot for 1, 2, 3 σ values of $\sin^2\theta_{12}$ in the parameter space $\sin^2\theta_{13}$ - $\cos\delta_{CP}$ according to the values for the NH in Table 1. The Orange and Red regions refers to the data at 2 σ and 3 σ , respectively. No region corresponding to the data at 1 σ is present.

We analyze quantitatively the expressions in eq. (2.45) and their correlation in Fig. 9(a), where $c_{12,13}^e$ have been taken as random complex numbers with absolute value following a Gaussian distribution around 1 with variance 0.5, while $\xi = 0.172$. In Fig. 9(b), we analyze the specific case $c_{13}^e = 0$, where $\xi = 0.18$ and $\cos\delta_{CP} = -1$. In Fig. 9, only the NH case is shown. The IH case is similar. Comparing Fig. 7(a) with Figs. 2 and 5, we can see that these S_4 models are strongly disfavoured with respect to the A_4 ones, and especially with respect to the special A_4 models.

In conclusion, from the point of view of reproducing the observed values of the mixing angles in a natural way, the A_4 models of the Lin type provide a most efficient solution. In the next sections we will study the performance of the different models for LFV processes.

3 Lepton Flavour Violation

In this section we discuss the implications on LFV processes of the three classes of models described in the previous section. In particular, given the stringent upper bound on $BR(\mu \rightarrow e\gamma)$, we focus on radiative lepton decays. By working in the super-CKM basis, where all kinetic terms are canonical and lepton mass matrices have been diagonalized through unitary transformations acting on the whole supermultiplets, the only sources of

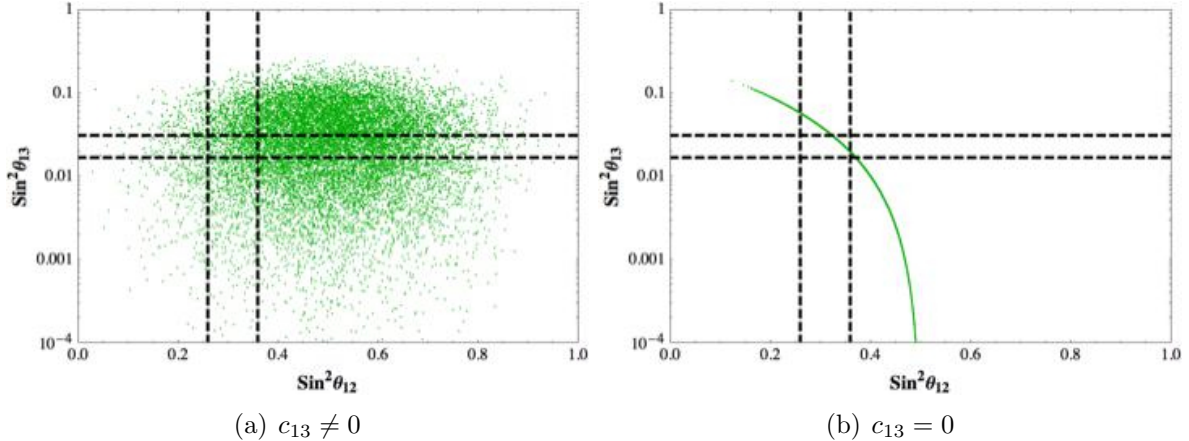


Figure 9: **S_4 Models.** $\sin^2 \theta_{13}$ as a function of $\sin^2 \theta_{12}$ is plotted, following eq. (2.45). The dashed-black lines represent the 3σ values for the mixing angles from the Fogli *et al.* fit [7]. Only the NH data sets is shown. On the left, the parameters c_{ij}^e are random complex numbers with absolute values following a Gaussian distribution around 1 with variance 0.5, while $\xi = 0.172$. In the right, $c_{13}^e = 0$, $\xi = 0.18$ and $\cos \delta_{CP} = -1$.

LFV are the off-diagonal terms of the slepton mass matrices. In our models these terms are much smaller than the corresponding diagonal entries and we can use the mass-insertion (MI) approximation [79–81] to illustrate the qualitative behavior of the model predictions. The quantitative results shown in our plots have been obtained by using complete one-loop results, which can be found for example in Refs. [82–88]. The normalized branching ratios R_{ij} for the LFV transitions $l_i \rightarrow l_j \gamma$

$$R_{ij} = \frac{BR(l_i \rightarrow l_j \gamma)}{BR(l_i \rightarrow l_j \nu_i \bar{\nu}_j)} \quad (3.1)$$

can be written as

$$R_{ij} = \frac{48\pi^3 \alpha}{G_F^2 m_{SUSY}^4} (|A_L^{ij}|^2 + |A_R^{ij}|^2) . \quad (3.2)$$

At the LO in the MI approximation, the amplitudes A_L^{ij} and A_R^{ij} are given by:

$$\begin{aligned} A_L^{ij} &= a_{LL}(\delta_{ij})_{LL} + a_{RL} \frac{m_{SUSY}}{m_i} (\delta_{ij})_{RL} \\ A_R^{ij} &= a_{RR}(\delta_{ij})_{RR} + a_{LR} \frac{m_{SUSY}}{m_i} (\delta_{ij})_{LR} \end{aligned} \quad (3.3)$$

where m_i are the charged fermion masses and $a_{CC'}$ ($C, C' = L, R$) are dimensionless functions of the SUSY parameters m_{SUSY} , $M_{1,2}$, μ , $\tan \beta$, renormalized at the electroweak scale. Here a common value in the diagonal entries of both LL and RR blocks of the slepton mass matrices has been assumed at the electroweak scale and m_{SUSY} denotes the average mass. Such assumption, often made at the cut-off scale in constrained versions of the MSSM, is spoiled by running effects and does not hold any more at the electroweak scale. We will

discuss this effect in the next subsection. The simplified framework considered here is sufficient to correctly describe the relation between R_{ij} and the expansion parameters ξ and ξ' . In our conventions the explicit expression of $a_{CC'}$ is given in appendix A. Their typical size is one tenth of $g^2/(16\pi^2)$, g being the $SU(2)_L$ gauge coupling constant. To appreciate the relative weights of the contributions in eq. (3.3), we list in Tab. 3 the expressions and the numerical values of the functions $a_{CC'}$, in the limit $\mu = M_{1,2} = m_{SUSY}$. As one can see, in this limit the dominant coefficient is a_{LL} , which is larger than $a_{RL} = a_{LR}$ by a factor $7 \div 54$, and larger than a_{RR} by a factor $4 \div 14$, depending on $\tan \beta = 2 \div 15$. This range of $\tan \beta$ is taken as representative for the models under consideration. More precisely, the parameter $\tan \beta$ is related to the expansion parameter η , the mass of the τ lepton and the τ Yukawa coupling y_τ , by:

$$\tan \beta \approx \frac{|y_\tau| \eta v_{EW}}{\sqrt{2} m_\tau}, \quad (3.4)$$

where $v_{EW} \approx 246$ GeV is the EW Higgs VEV. For typical A_4 models the parameter $\eta \approx \xi$ is of order 0.1. For special A_4 model, $\eta \approx \xi$ is smaller than ξ' and we will use the range $0.007 \lesssim \eta \lesssim 0.05$. For the S_4 models, we have $\eta \approx 0.08$ to correctly fit the charged lepton masses. Requiring y_τ to be of order one, $1/3 \lesssim |y_\tau| \lesssim 3$, we have the following allowed ranges for $\tan \beta$:

$$\begin{aligned} 3 \lesssim \tan \beta \lesssim 30 & \quad \text{Typical } A_4 \\ 2 \lesssim \tan \beta \lesssim 15 & \quad \text{Special } A_4 \\ 3 \lesssim \tan \beta \lesssim 24 & \quad S_4 \end{aligned} \quad (3.5)$$

a_{LL}	$\frac{1}{240} \frac{g^2}{16\pi^2} \left[1 - 3(1+4c) \tan^2 \theta_W + 4(4+5 \tan^2 \theta_W) \tan \beta \right]$	$+(2.0 \div 16.3)$
$a_{RL} = a_{LR}$	$\frac{1}{12} \frac{g^2}{16\pi^2} \tan^2 \theta_W$	0.30
a_{RR}	$\frac{1}{60} \frac{g^2}{16\pi^2} \tan^2 \theta_W [-3 - 3c - \tan \beta]$	$-(0.5 \div 1.2)$

Table 3: Coefficients $a_{CC'}$ characterizing the transition amplitudes for $\mu \rightarrow e\gamma$, $\tau \rightarrow e\gamma$ and $\tau \rightarrow \mu\gamma$, in the MI approximation and by taking the limit the $\mu = M_{1,2} = m_{SUSY}$. Numerical values are given in units of $g^2/(192\pi^2)$ and using $\sin^2 \theta_W = 0.23$, $c = 1$, and $\tan \beta = 2 \div 15$. The parameter c is a model dependent quantity of order one.

Finally, $(\delta_{ij})_{CC'}$ parametrize the MIs and are defined as:

$$(\delta_{ij})_{CC'} = \frac{(\hat{m}_{eCC'}^2)_{ij}}{m_{SUSY}^2}, \quad (3.6)$$

where the different blocks of the slepton mass matrices $\hat{m}_{eCC'}^2$ are evaluated in the super-CKM basis, denoted by the hat. There are two main types of contributions to the MIs $(\delta_{ij})_{CC'}$: the first one comes from local operators, bilinear in the slepton fields, with insertions of the flavons $\Phi_{e,\nu}$. They are invariant under the flavour symmetry and represent

the counterpart, in the sparticle sector, of the operators that generate lepton masses in the theory. After the breaking of the flavour symmetry, we get slepton mass matrices expanded up to a certain order in $\langle\Phi_{e,\nu}\rangle/\Lambda$, depending on the highest dimensionality of the operators included:

$$\hat{m}^2 = \hat{m}_0^2 + \delta\hat{m}_1^2 + \delta\hat{m}_2^2 + \dots \quad (3.7)$$

with $\delta\hat{m}_p^2$ of order $(\langle\Phi_{e,\nu}\rangle/\Lambda)^p$.

The second contribution to the MIs in eq. (3.6) comes from the renormalization group evolution (RGE). When neutrino masses are generated by the See-Saw mechanism, the evolution spans two main regions. The first one goes from the cut-off scale Λ where slepton masses are generated⁷, down to the lightest right-handed neutrino mass M_1 . In our models the mass scale associated to right-handed neutrinos coincides with the flavour symmetry breaking scale $\langle\Phi_\nu\rangle$ and, in a leading logarithmic approximation, we get a contribution to the MIs proportional to $y^2/(16\pi^2) \times \log(\langle\Phi_\nu\rangle/\Lambda)$, y representing a typical neutrino Yukawa coupling. Below M_1 the right-handed neutrinos decouple and the running is only affected by the lightest degrees of freedom, those of the MSSM. This part of the RGE occurs whether or not neutrino masses originate from the See-Saw mechanism and gives rise to contributions to the MIs proportional to $y_\tau^2/(16\pi^2) \times \log(\langle\Phi_\nu\rangle/m_{SUSY})$, y_τ denoting the τ Yukawa coupling.

We now discuss in turn the different contributions to the MIs for the three classes of models.

3.1 Mass Insertions from Local Operators

Local operators giving rise to slepton masses can be constructed with standard techniques, see Refs. [89–100]. The inclusion of non-renormalizable operators with insertions of the flavon fields $\Phi_{e,\nu}$ also affects kinetic terms both in the fermion and sfermion sector, providing an additional source of flavour violation. Here we list the slepton mass matrices in the super-CKM basis where kinetic terms have been set in the canonical form by means of appropriate transformations and where fermion mass matrices have been made diagonal through unitary transformations acting on the whole supermultiplet. These slepton masses refer to specific models, taken as representative of the classes analyzed above. For typical A_4 models we will refer to the construction in Ref. [71], for special A_4 models we will consider the model of Ref. [61] and finally S_4 models are exemplified by the model in Ref. [52]. The results given below have been obtained under the assumption that the underlying parameters are real.

⁷Depending on the specific type of SUSY breaking mechanism slepton mass generation can occur at a scale smaller than Λ . Here we assume that slepton masses are produced at the highest scale, like in gravity mediated SUSY breaking scenarios.

3.1.1 Typical A_4 Models

For typical A_4 models we get

$$\hat{m}_{LL}^2 = \begin{pmatrix} 1 + \mathcal{O}(\xi) & \mathcal{O}(\xi^2) & \mathcal{O}(\xi^2) \\ \mathcal{O}(\xi^2) & 1 + \mathcal{O}(\xi) & \mathcal{O}(\xi^2) \\ \mathcal{O}(\xi^2) & \mathcal{O}(\xi^2) & 1 + \mathcal{O}(\xi) \end{pmatrix} m_{SUSY}^2 + \dots \quad (3.8)$$

$$\hat{m}_{RR}^2 = \begin{pmatrix} \mathcal{O}(1) & \frac{m_e}{m_\mu} \mathcal{O}(\xi) & \frac{m_e}{m_\tau} \mathcal{O}(\xi) \\ \frac{m_e}{m_\mu} \mathcal{O}(\xi) & \mathcal{O}(1) & \frac{m_\mu}{m_\tau} \mathcal{O}(\xi) \\ \frac{m_e}{m_\tau} \mathcal{O}(\xi) & \frac{m_\mu}{m_\tau} \mathcal{O}(\xi) & \mathcal{O}(1) \end{pmatrix} m_{SUSY}^2 + \dots \quad (3.9)$$

$$\hat{m}_{RL}^2 = \begin{pmatrix} \mathcal{O}(m_e) & m_e \mathcal{O}(\xi) & m_e \mathcal{O}(\xi) \\ m_\mu \mathcal{O}(\xi^2) & \mathcal{O}(m_\mu) & m_\mu \mathcal{O}(\xi) \\ m_\tau \mathcal{O}(\xi^2) & m_\tau \mathcal{O}(\xi^2) & \mathcal{O}(m_\tau) \end{pmatrix} m_{SUSY} + \dots \quad (3.10)$$

where dots stand for negligible SUSY contributions. In \hat{m}_{RL}^2 we have neglected a contribution which arises if the F component of the flavon supermultiplets acquires a VEV. Such a contribution depends on the SUSY breaking mechanism and vanishes under mild assumptions [96, 101, 102]. A similar contribution will be neglected also in the special A_4 and in the S_4 models discussed below. We have

$$\begin{aligned} (\delta_{ij})_{LL} &= \mathcal{O}(\xi^2), & (\delta_{ij})_{RL} &= \frac{m_i}{m_{SUSY}} \mathcal{O}(\xi^2), \\ (\delta_{ij})_{RR} &= \frac{m_j}{m_i} \mathcal{O}(\xi), & (\delta_{ij})_{LR} &= \frac{m_j}{m_{SUSY}} \mathcal{O}(\xi), \end{aligned} \quad (3.11)$$

and

$$\begin{aligned} A_L^{ij} &= a_{LL} \mathcal{O}(\xi^2) + a_{RL} \mathcal{O}(\xi^2), \\ A_R^{ij} &= a_{RR} \frac{m_j}{m_i} \mathcal{O}(\xi) + a_{RL} \frac{m_j}{m_i} \mathcal{O}(\xi). \end{aligned} \quad (3.12)$$

From $\xi \approx 0.1$ and the numerical values of $a_{CC'}$ we see that the amplitude A_L^{ij} is the dominant one. We approximately have

$$R_{ij} \simeq \frac{48\pi^3 \alpha}{G_F^2 m_{SUSY}^4} |a_{LL} + a_{RL}|^2 \mathcal{O}(\xi^4), \quad (3.13)$$

and we expect the branching ratios of the three transitions to be of the same order of magnitude:

$$R_{\mu e} \approx R_{\tau\mu} \approx R_{\tau e}, \quad (3.14)$$

at variance with the predictions of most of the other models, where, for instance, $R_{\mu e}/R_{\tau\mu}$ can be much smaller than one [103–106].

3.1.2 Special A_4 Models

For the special A_4 model in Ref. [61] we get :

$$\hat{m}_{LL}^2 = \begin{pmatrix} 1 + \mathcal{O}(\xi'^2) & \mathcal{O}(\xi'^2) & \mathcal{O}(\xi'^2) \\ \mathcal{O}(\xi'^2) & 1 + \mathcal{O}(\xi'^2) & \mathcal{O}(\xi'^2) \\ \mathcal{O}(\xi'^2) & \mathcal{O}(\xi'^2) & 1 + \mathcal{O}(\xi'^2) \end{pmatrix} m_{SUSY}^2 + \dots \quad (3.15)$$

$$\hat{m}_{RR}^2 = \begin{pmatrix} \mathcal{O}(1) & \frac{m_e}{m_\mu} \mathcal{O}(\xi'^2) & \mathcal{O}(\xi'^3) \\ \frac{m_e}{m_\mu} \mathcal{O}(\xi'^2) & \mathcal{O}(1) & \frac{m_\mu}{m_\tau} \mathcal{O}(\xi'^2) \\ \mathcal{O}(\xi'^3) & \frac{m_\mu}{m_\tau} \mathcal{O}(\xi'^2) & \mathcal{O}(1) \end{pmatrix} m_{SUSY}^2 + \dots \quad (3.16)$$

$$\hat{m}_{RL}^2 = \begin{pmatrix} \mathcal{O}(m_e) & m_e \mathcal{O}(\xi'^2) & m_e \mathcal{O}(\xi'^2) \\ m_\mu \mathcal{O}(\xi'^2) & \mathcal{O}(m_\mu) & m_\mu \mathcal{O}(\xi'^2) \\ m_\tau \mathcal{O}(\xi'^2) & m_\tau \mathcal{O}(\xi'^2) & \mathcal{O}(m_\tau) \end{pmatrix} m_{SUSY} + \dots \quad (3.17)$$

We have

$$\begin{aligned} (\delta_{ij})_{LL} &= \mathcal{O}(\xi'^2), \\ (\delta_{21})_{RR} &= \frac{m_e}{m_\mu} \mathcal{O}(\xi'^2) & (\delta_{32})_{RR} &= \frac{m_\mu}{m_\tau} \mathcal{O}(\xi'^2) & (\delta_{31})_{RR} &= \mathcal{O}(\xi'^3), \\ (\delta_{ij})_{RL} &= \frac{m_i}{m_{SUSY}} \mathcal{O}(\xi'^2) & (\delta_{ij})_{LR} &= \frac{m_j}{m_{SUSY}} \mathcal{O}(\xi'^2) \end{aligned} \quad (3.18)$$

and

$$\begin{aligned} A_L^{ij} &= a_{LL} \mathcal{O}(\xi'^2) + a_{RL} \mathcal{O}(\xi'^2), \\ A_R^{ij} &= \begin{cases} a_{RR} \frac{m_j}{m_i} \mathcal{O}(\xi'^2) + a_{RL} \frac{m_j}{m_i} \mathcal{O}(\xi'^2) & (ij = 21, 32) \\ a_{RR} \mathcal{O}(\xi'^3) + a_{RL} \frac{m_j}{m_i} \mathcal{O}(\xi'^2) & (ij = 31). \end{cases} \end{aligned} \quad (3.19)$$

Neglecting the subdominant contribution from the A_R^{ij} amplitude, we have

$$R_{ij} \simeq \frac{48\pi^3 \alpha}{G_F^2 m_{SUSY}^4} |a_{LL} + a_{RL}|^2 \mathcal{O}(\xi'^4), \quad (3.20)$$

and we expect the branching ratios of the three transitions to be of the same order of magnitude:

$$R_{\mu e} \approx R_{\tau\mu} \approx R_{\tau e}. \quad (3.21)$$

3.1.3 S_4 Models

For S_4 models we get:

$$\hat{m}_{LL}^2 = \begin{pmatrix} 1 + \mathcal{O}(\xi) & \mathcal{O}(\xi) & \mathcal{O}(\xi) \\ \mathcal{O}(\xi) & 1 + \mathcal{O}(\xi) & \mathcal{O}(\xi^2) \\ \mathcal{O}(\xi) & \mathcal{O}(\xi^2) & 1 + \mathcal{O}(\xi) \end{pmatrix} m_{SUSY}^2 + \dots \quad (3.22)$$

$$\hat{m}_{RR}^2 = \begin{pmatrix} \mathcal{O}(1) & \frac{m_e}{m_\mu} \mathcal{O}(\xi) & \frac{m_e}{m_\tau} \mathcal{O}(\xi) \\ \frac{m_e}{m_\mu} \mathcal{O}(\xi) & \mathcal{O}(1) & \frac{m_\mu}{m_\tau} \mathcal{O}(\xi^2) \\ \frac{m_\mu}{m_e} \mathcal{O}(\xi) & \frac{m_\mu}{m_\tau} \mathcal{O}(\xi^2) & \mathcal{O}(1) \end{pmatrix} m_{SUSY}^2 + \dots \quad (3.23)$$

$$\hat{m}_{RL}^2 = \begin{pmatrix} \mathcal{O}(m_e) & m_e \mathcal{O}(\xi) & m_e \mathcal{O}(\xi) \\ m_\mu \mathcal{O}(\xi) & \mathcal{O}(m_\mu) & m_\mu \mathcal{O}(\xi^2) \\ m_\tau \mathcal{O}(\xi) & m_\tau \mathcal{O}(\xi^2) & \mathcal{O}(m_\tau) \end{pmatrix} m_{SUSY}^2 + \dots \quad (3.24)$$

We have

$$\begin{aligned} (\delta_{ij})_{LL} &= \mathcal{O}(\xi^p), & (\delta_{ij})_{RL} &= \frac{m_i}{m_{SUSY}} \mathcal{O}(\xi^p), \\ (\delta_{ij})_{RR} &= \frac{m_j}{m_i} \mathcal{O}(\xi^p), & (\delta_{ij})_{LR} &= \frac{m_j}{m_{SUSY}} \mathcal{O}(\xi^p) \end{aligned} \quad (3.25)$$

where $p = 1$ when $ij = 21, 31$ and $p = 2$ when $ij = 32$

$$\begin{aligned} A_L^{ij} &= a_{LL} \mathcal{O}(\xi^p) + a_{RL} \mathcal{O}(\xi^p), \\ A_R^{ij} &= a_{RR} \frac{m_j}{m_i} \mathcal{O}(\xi^p) + a_{RL} \frac{m_j}{m_i} \mathcal{O}(\xi^p). \end{aligned} \quad (3.26)$$

Neglecting the subdominant contribution from the A_R^{ij} amplitude, we have

$$R_{ij} \simeq \frac{48\pi^3 \alpha}{G_F^2 m_{SUSY}^4} |a_{LL} + a_{RL}|^2 \times \begin{cases} \mathcal{O}(\xi^2) & (ij = 21, 31) \\ \mathcal{O}(\xi^4) & (ij = 32), \end{cases} \quad (3.27)$$

with a suppression of the rate $\tau \rightarrow \mu\gamma$ relative to $\mu \rightarrow e\gamma$ and $\tau \rightarrow e\gamma$ by a factor of ξ^2 :

$$R_{\tau\mu} \ll R_{\mu e} \approx R_{\tau e}. \quad (3.28)$$

Before a more quantitative illustration of these results, we discuss the effects induced by the RGE from the scale of flavour symmetry breaking down to the electroweak scale.

3.2 Mass Insertions from low-energy RGE

This set of corrections is common to all models irrespective of the assumed existence of RH neutrinos, i.e. both with or without See-Saw. The running of the slepton mass parameters from the scale $\langle \Phi_{e,\nu} \rangle$ down to the scale m_{SUSY} can be estimated in a leading logarithmic approximation. The largest effect is a correction to the matrices \hat{m}_{LL}^2 and \hat{m}_{RR}^2 coming from electroweak gauge interactions and is proportional to the identity matrix in flavour space. One finds that the diagonal elements increase in the running from the cutoff scale down to the electroweak scale. This effect is taken into account in our numerical study. As for the off diagonal entries the largest corrections are proportional to the square of the τ Yukawa coupling. Since $y_\tau^2/(16\pi^2) \approx 3 \times (10^{-6} \div 10^{-4})$ for $\tan \beta = (2 \div 15)$, even in the presence of the large factor $\log(\langle \Phi_{e,\nu} \rangle / m_{SUSY}) \approx 30$, these corrections are negligibly small compared to the contribution from the local operators discussed above. We can

conclude that the corrections to the off-diagonal entries of the soft mass matrices induced by the RGE from $\langle \Phi_{e,\nu} \rangle$ down to m_{SUSY} are either negligible or could be absorbed in the parametrization given in the previous section.

The present bound on the branching ratio of $\mu \rightarrow e\gamma$ from the MEG collaboration [64], $BR(\mu \rightarrow e\gamma) < 2.4 \times 10^{-12}$, leads to strong constraints on the parameter space of the models that we are considering in this work. The supersymmetric parameters that are not constrained by the flavour symmetry, such as the soft SUSY mass scales and the gaugino and Higgs(ino) sectors, are fixed by our choice of a SUGRA framework: m_0 and $M_{1/2}$ are the common masses of scalar particles and gauginos at the GUT scale. Thus, at the scale $\Lambda = 2 \times 10^{16}$ GeV,

$$M_1(\Lambda) = M_2(\Lambda) = M_{1/2}, \quad (3.29)$$

where M_i are the $SU(2) \times U(1)$ gaugino masses. The effects of the RG running lead at low energies to the following masses for the gauginos

$$M_1(m_W) \simeq \frac{\alpha_1(m_W)}{\alpha_1(\Lambda)} M_1(\Lambda) \quad M_2(m_W) \simeq \frac{\alpha_2(m_W)}{\alpha_2(\Lambda)} M_2(\Lambda), \quad (3.30)$$

where $\alpha_i = g_i^2/4\pi$ ($i = 1, 2$) and $\alpha_1(\Lambda) = \alpha_2(\Lambda) \simeq 1/25$. We have seen that, among the RG running effects on the soft mass terms, only those from the electroweak gauge interactions are relevant. At the cut-off scale the LL and RR blocks of the slepton mass matrices are given by the eqs. (3.8)-(3.10), (3.15)-(3.17) and (3.22)-(3.24) with m_{SUSY} identified with m_0 . The RGE due to electroweak gauge interactions leaves the off-diagonal entries essentially unaffected, while the diagonal elements at the weak scale, denoted by $m_{L,R}^2(m_W)$, are given by:

$$\begin{aligned} m_L^2(m_W) &\simeq m_0^2 + 0.54 M_{1/2}^2, \\ m_R^2(m_W) &\simeq m_0^2 + 0.15 M_{1/2}^2. \end{aligned} \quad (3.31)$$

Notice that this effect modifies the previous estimates of the $LL(RR)$ MIs by a factor $m_0^2/(m_0^2 + 0.54(0.15)M_{1/2}^2)$, thus providing an additional suppression when $M_{1/2}$ is larger than m_0 .

Furthermore, the parameter μ is fixed through the requirement of correct electroweak symmetry breaking⁸

$$|\mu|^2 \simeq -\frac{m_Z^2}{2} + m_0^2 \frac{1 + 0.5 \tan^2 \beta}{\tan^2 \beta - 1} + M_{1/2}^2 \frac{0.5 + 3.5 \tan^2 \beta}{\tan^2 \beta - 1}, \quad (3.33)$$

so that μ is determined by m_0 , $M_{1/2}$ and $\tan \beta$ up to its sign. We recall that in our model the low energy parameter $\tan \beta$ is not a free parameter, as shown in Eq. (3.4). We compare the models at $\tan \beta = 2$ and $\tan \beta = 15$. In our numerical analysis, we have assumed

⁸The general definition of the parameter μ is

$$|\mu|^2 = \frac{m_{H_d}^2 - m_{H_u}^2 \tan^2 \beta}{\tan^2 \beta - 1} - \frac{1}{2} m_Z^2, \quad (3.32)$$

that reduces to the expression in Eq. (3.33) once considering that in the SUGRA framework the soft Higgs mass parameters are also given by m_0 at the high energy scale, $m_{H_u}^2(\Lambda) = m_{H_d}^2(\Lambda) = m_0^2$.

that the parameters on the diagonal of the slepton mass matrices $(m_{(e,\nu)LL}^2)_K$ and $(m_{eRR}^2)_K$ are positive in order to get positive definite square-masses and to avoid electric-charge breaking minima and further sources of electroweak symmetry breaking. The absolute value of the $\mathcal{O}(1)$ parameters is varied between 1/2 and 2. Furthermore, we have imposed the conditions that the lightest chargino has a mass larger than 100 GeV and that the lightest neutralino is the lightest supersymmetric a particle (LSP).

The results for the typical A_4 models are illustrated in Fig. 10, where the parameter ξ is taken equal to 0.076, consistently with the analysis in Sec. 2.1.1. For $\tan\beta = 2$ and $m_0 = 200$ GeV, Fig. 10(a), almost all the points are excluded for $M_{1/2} \lesssim 400$ GeV. The corresponding supersymmetric spectrum is rather light: for $M_{1/2} = 400$ GeV, the lightest neutralino has a mass of ~ 156 GeV, the lightest chargino of ~ 306 GeV, the lightest LH charged slepton is in the range [230, 500] GeV and the lightest RH charged slepton in the range [160, 350] GeV. These mass values are not yet excluded by the LHC (the limits in the EW sector are not very strong) and they only mark the lower edge of the region allowed by the $\mu \rightarrow e\gamma$ bounds. Increasing m_0 up to 5000 GeV, Fig. 10(b), we see that the MEG bound is well satisfied in this model for the whole plotted range of $M_{1/2}$. The corresponding supersymmetric spectrum is heavier: again for $M_{1/2} = 400$ GeV, while the lightest neutralino and chargino have masses very similar to the previous case, ~ 158 GeV and ~ 315 GeV, respectively, the lightest LH and RH charged slepton masses are much higher, being in the range [3850, 7070] GeV and [1800, 6260] GeV, respectively. Increasing m_0 from 200 GeV up to 5000 GeV does not correspond to a uniform decrease of the branching ratio, as a function of $M_{1/2}$. The plot with $m_0 = 5000$ GeV is much flatter compared to the plot where $m_0 = 200$ GeV. This is due to the approximate factor $m_0^2/(m_0^2 + 0.54M_{1/2}^2)$ entering the dominant LL mass insertion, which, for the values of $M_{1/2}$ used in our plots, is sharply decreasing for $m_0 = 200$ GeV while it is slowly varying and close to one for $m_0 = 5000$ GeV. This is a general feature reproduced by all the models considered here.

Increasing the value of $\tan\beta$, Figs. 10(c)-(d), the number of points below the MEG bound decreases, but the previous considerations are approximately still valid: in particular notice that for $m_0 = 5000$ GeV, there are always points satisfying the MEG bound, even if the largest number of them falls in the excluded region, especially for smaller $M_{1/2}$. Since the dominant contribution to the branching ratio comes from the LL mass insertion which is proportional to $\tan\beta$, the branching ratio is to a good approximation proportional to $\tan^2\beta$, as we can see from the plots. Also this feature is common to all models.

For special A_4 models the parameter ξ' is taken equal to 0.184, as analyzed in Sec. 2.1.2. The results of our numerical study considering the constraint from $BR(\mu \rightarrow e\gamma)$ for the $m_0 - M_{1/2}$ parameter space are shown in Fig. 11. The plots in Fig. 11 are very similar to those in Fig. 10. Indeed also for this case, for $\tan\beta = 2$ and $m_0 = 200$ GeV, Fig. 11(a), almost all the points are excluded for $M_{1/2} \lesssim 400$ GeV. The supersymmetric spectrum is also quite similar: the only differences are in the range of masses that the lightest LH and RH charged sleptons can span, [260, 500] GeV and [180, 340] GeV, respectively. By increasing m_0 up to 5000 GeV, Fig. 10(b), we can see that for the whole range of $M_{1/2}$, the MEG bound is well satisfied in this model, while the corresponding supersymmetric spectrum is heavier. Special and typical A_4 models have a dominant LL mass insertion

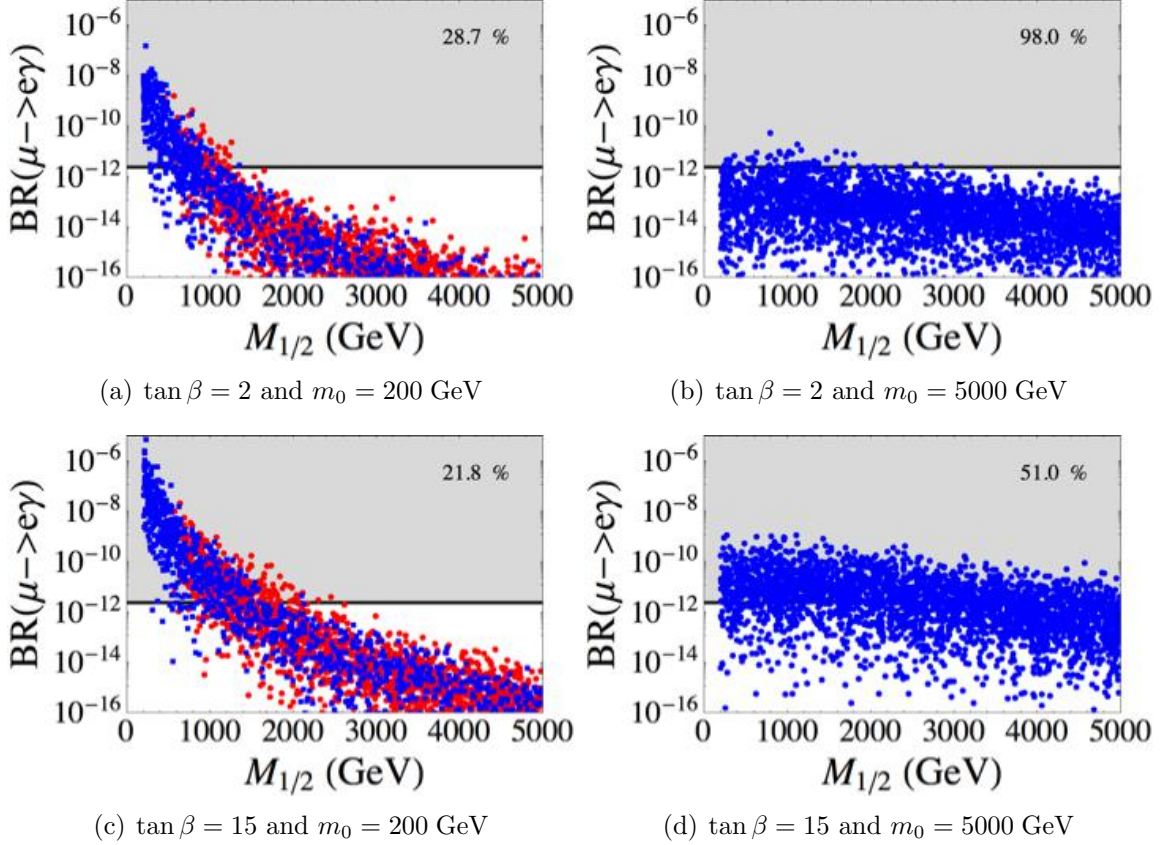


Figure 10: **Typical A_4 Models.** Scatter plots of $BR(\mu \rightarrow e\gamma)$ as a function of $M_{1/2}$, for different values of $\tan \beta$, and m_0 . The parameter ξ is chosen as 0.076 in order to maximize the success rate of this model. The horizontal line shows the current MEG bound. For Blue (Red) points the LSP is the lightest neutralino (stau). The percentage in each plot refers to the number of Blue points that satisfy the MEG bound over the total number of points.

proportional to ξ'^2 and ξ^2 , respectively, which represents the main difference between the two models, as far as radiative charged lepton decays are considered. The optimal values of ξ and $|\xi'|$ differ by a factor of about two and we expect that the branching ratios of the two models should differ by about one order of magnitude, for fixed values of the other parameters. This effect is barely visible in our plots, due to the spread of the predictions caused by the unknown order-one coefficients.

Increasing the value of $\tan \beta$, the number of points below the MEG bound decreases, but the previous consideration are approximatively still valid: the most interesting difference is in Fig. 11(c), for $m_0 = 200$ GeV, where almost all the points with $M_{1/2} < 1000$ GeV are excluded; furthermore, in Fig. 11(d), for $m_0 = 5000$ GeV, there are always points satisfying the MEG bound, even if the largest part are excluded, especially for smaller $M_{1/2}$.

Finally, in the S_4 model the parameter ξ is taken equal to 0.172, as required to maximize the success rate of these models to arrange the three mixing angles in the corresponding 3σ ranges. The results are displayed in Fig. 12. The plots in Fig. 12 are very similar to

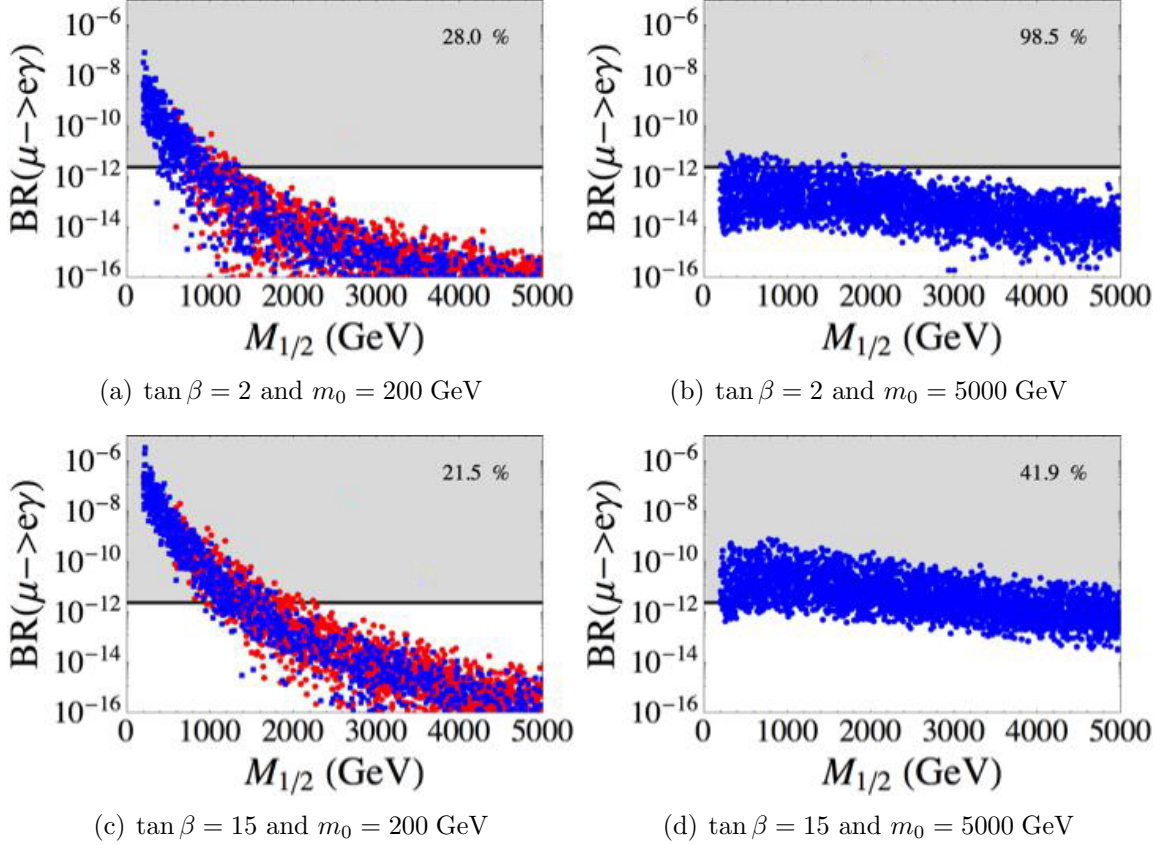


Figure 11: **Special A_4 Models.** Scatter plots of $BR(\mu \rightarrow e\gamma)$ as a function of $M_{1/2}$, for different values of $\tan \beta$, and m_0 . The parameter $|\xi'|$ is chosen as 0.184 in order to maximize the success rate of this model. The horizontal line shows the current MEG bound. For Blue (Red) points the LSP is the lightest neutralino (stau). The percentage in each plot refers to the number of Blue points that satisfy the MEG bound over the total number of points.

those in Fig. 11 and the same comments also apply here. More interestingly, in all the plots the number of points satisfying the MEG bound is much smaller, especially for large m_0 . In particular for $\tan \beta = 15$ and $m_0 = 5000$ GeV, only the $\sim 10\%$ of points correspond to a BR smaller than the MEG bound. The relatively larger branching ratio for $\mu \rightarrow e\gamma$ predicted by the S_4 model is also a consequence of the scaling of $(\delta_{\mu e})_{LL}$ with respect to ξ : such a scaling is linear in S_4 , while it is quadratic in the typical A_4 models. Moreover the optimal value of ξ in S_4 is larger than in typical A_4 models. This explains the enhancement by two order of magnitude of the S_4 prediction compared to the typical A_4 one.

3.3 Mass Insertion from high-energy RGE

When neutrino masses originate from a Type I See-Saw mechanism, there is an extra contribution to the running of the slepton mass matrices, originating from loop diagrams with the exchange of right-handed neutrinos. Such a contribution is only relevant in the

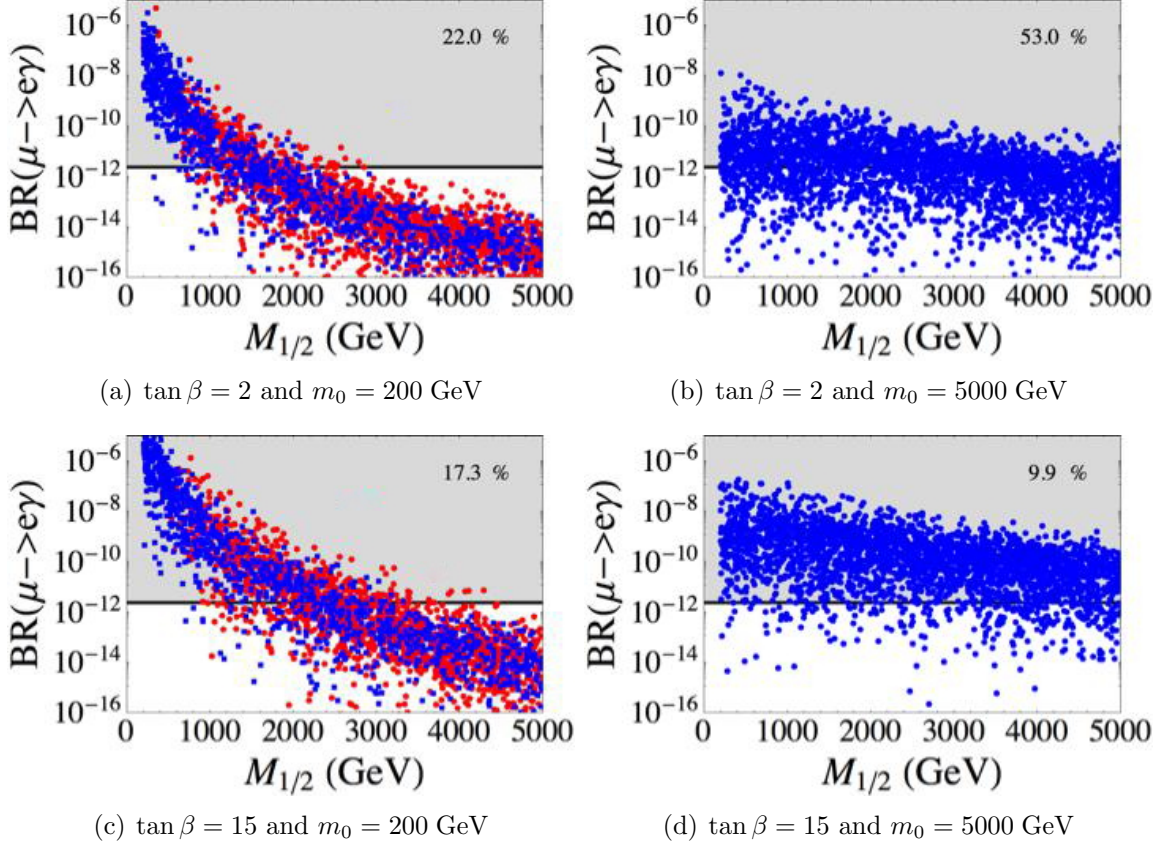


Figure 12: **\mathcal{S}_4 Models.** Scatter plots of $BR(\mu \rightarrow e\gamma)$ as a function of $M_{1/2}$, for different values of $\tan\beta$, and m_0 . The parameter ξ is chosen as 0.172 in order to maximize the success rate of this model. The horizontal line shows the current MEG bound. For Blue (Red) points the LSP is the lightest neutralino (stau). The percentage in each plot refers to the number of Blue points that satisfy the MEG bound over the total number of points.

energy range from the cut-off Λ of the theory down to the right-handed neutrino masses M_k ($k = 1, 2, 3$). By focussing on the LL block m_{eLL}^2 of the slepton mass matrix, whose non-diagonal entries dominate the rates of the processes under consideration, in the leading log approximation we have [107–109]

$$(m_{eLL}^2)_{ij} \simeq -\frac{1}{8\pi^2} (3m_0^2 + A_0^2) \sum_k (\hat{Y}_\nu^\dagger)_{ik} \log\left(\frac{\Lambda}{M_k}\right) (\hat{Y}_\nu)_{kj}, \quad (3.34)$$

where A_0 is the SUSY breaking parameter characterizing the size of the trilinear scalar mass term for sleptons and the matrix \hat{Y}_ν denotes the neutrino Yukawa couplings in the basis where the mass matrices for charged leptons and right-handed neutrinos have been diagonalized. The above expression for m_{eLL}^2 holds at the scale equal to the lightest right-handed neutrino mass. Below that scale, right-handed neutrinos do not affect the running any more. In the models we are considering neutrino Yukawa couplings are of order one and even for relatively small ratios $\Lambda/M_K \approx 100$, we may easily get contributions to the LL mass insertions of order 0.1.

It is interesting to note that if neutrinos transform as an irreducible triplet of the flavour symmetry then, at the LO in the flavour symmetry breaking parameters, the right-hand side of eq. (3.34) can be expressed in term of the light neutrino masses and the matrix elements of the lepton mixing matrix U . We have

$$\hat{Y}_\nu = k U^\dagger + \dots \quad (3.35)$$

and

$$(m_{eLL}^2)_{ij} \simeq -\frac{|k|^2}{8\pi^2} (3m_0^2 + A_0^2) \left[U_{i2} \log \frac{m_2}{m_1} U_{j2}^* + U_{i3} \log \frac{m_3}{m_1} U_{j3}^* \right] + \dots, \quad (3.36)$$

where k is a constant of order one and dots stand for non-leading contributions, suppressed by powers of $\langle \Phi \rangle / \Lambda$. This result is completely general. It applies to any model with a flavour symmetry, independently of the specific flavour group G_f , provided neutrinos are assigned to an irreducible triplet of the group, like in the models under consideration. First note that the invariance of the theory under transformations of G_f implies

$$\rho(g) Y_\nu^\dagger Y_\nu \rho(g)^\dagger = Y_\nu^\dagger Y_\nu, \quad (3.37)$$

ρ denoting the irreducible triplet representation under which the left-handed leptons transform. The combination $Y_\nu^\dagger Y_\nu$ commutes with each group element $\rho(g)$ and, by the Shur's First Lemma, $Y_\nu^\dagger Y_\nu$ either vanishes, a case that we exclude, or is proportional to the unit matrix. We conclude that Y_ν is proportional to a unitary matrix. This result holds in any basis, since the invariance of the theory is a basis-independent property. If now we go to the basis where charged leptons and right-handed neutrinos are mass eigenstates, the See-Saw relation reads:

$$m_\nu = \frac{v^2}{2} \hat{Y}_\nu^T M^{-1} \hat{Y}_\nu \quad (3.38)$$

and we recognize that in this basis the unitary matrix to which \hat{Y}_ν is proportional should coincide with U^\dagger . We obtain eq. (3.35) and

$$M^{-1} = \frac{2}{|k|^2 v^2} (m_\nu)_{diag} \quad (3.39)$$

By making use of eqs. (3.35), (3.39) and (3.34) we immediately get the result in eq. (3.36). Thus, up to sub-leading corrections and up to the unknown order-one parameter k , the LL mass insertions are completely determined by neutrino masses and mixing parameters. At the LO the MIs do not depend on the cut-off scale Λ , but only on the ratios between light neutrino masses. For a degenerate neutrino spectrum the LO MIs vanish. On the contrary the largest MIs are obtained when the spectrum is hierarchical.

We have considered the type I See-Saw version of the previous models and we have evaluated the slepton mass matrices by including the effects on the running due to right-handed neutrinos. Our plots and our numerical results have been worked out at the NLO in the symmetry breaking parameters. RGE equations are solved numerically, making use of full one-loop beta functions. The evolution starts at $\Lambda = 2 \times 10^{16}$ GeV, where we assume the pattern dictated by the eqs. (3.8)-(3.10), (3.15)-(3.17) and (3.22)-(3.24) with m_{SUSY}

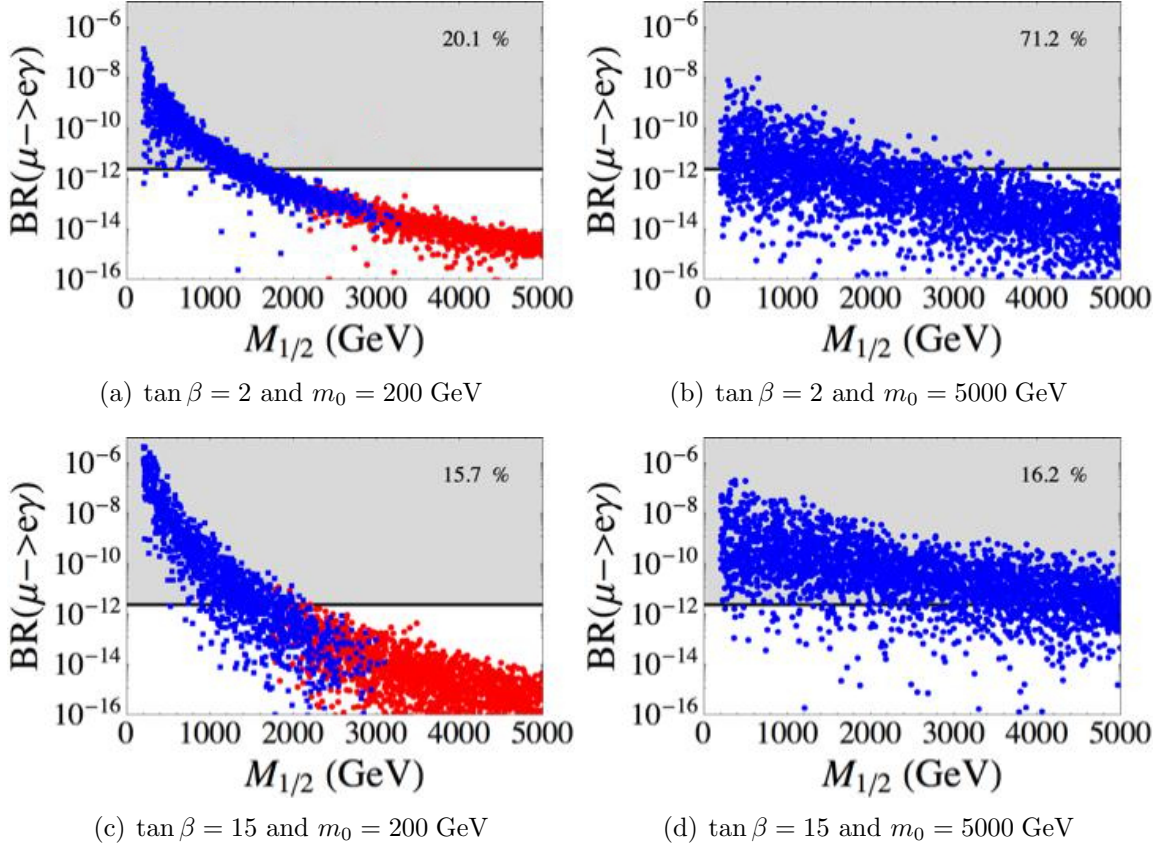


Figure 13: **Typical A_4 Models.** Scatter plots of $BR(\mu \rightarrow e\gamma)$ with running effects due to right-handed neutrinos, as a function of $M_{1/2}$, for different values of $\tan \beta$, and m_0 . Light neutrinos have normal mass ordering with $m_1 = 4.4$ meV. The parameter ξ is chosen as 0.076 in order to maximize the success rate of this model. The horizontal line shows the current MEG bound. For Blue (Red) points the LSP is the lightest neutralino (stau). The percentage in each plot refers to the number of Blue points that satisfy the MEG bound over the total number of points.

identified with m_0 . Going down to the electroweak scale the off-diagonal entries of the slepton mass matrices are modified by the running due to both right-handed neutrinos and by the MSSM degrees of freedom. We display our results for the case of normal ordering. Similar considerations hold when the neutrino mass ordering is inverted. For the lightest neutrino mass we chose the smallest value allowed by the models under consideration: 4.4 meV for the typical A_4 models, 0.4 meV for the special A_4 models and 1 meV for S_4 . These values can be estimated by analyzing the neutrino masses in the See-Saw version of the models in Refs. [71], [61] and [52], considered in the previous subsections. Choosing the smallest value of m_1 enhances the ratios m_2/m_1 and m_3/m_1 in eq. (3.36) and maximizes the effect of the running due to right-handed neutrinos.

In Figs. 13, 14 and 15 we plot the branching ratio for $\mu \rightarrow e\gamma$ as a function of $M_{1/2}$ for the same values of m_0 and $\tan \beta$ shown in Figs. 10, 11 and 12 to allow for a direct comparison between the two cases, with and without right-handed neutrinos. As a general

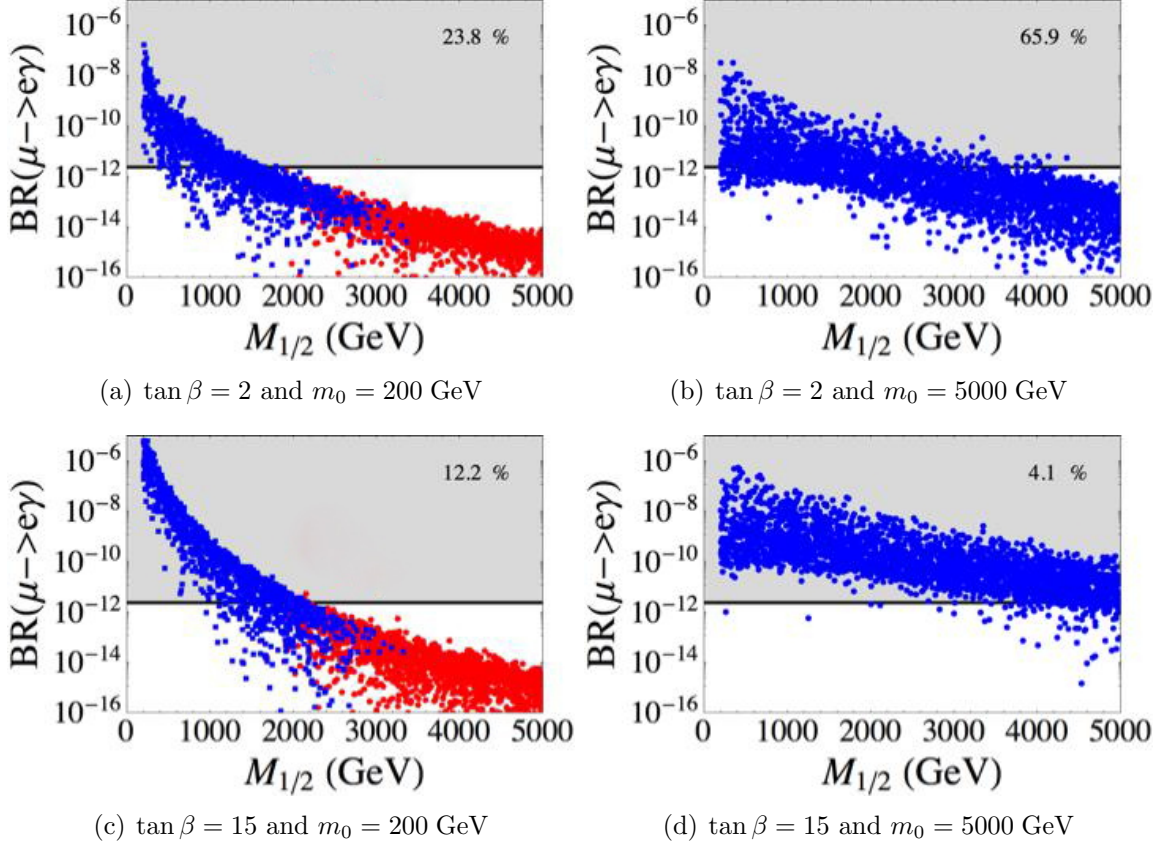


Figure 14: **Special A_4 Models.** Scatter plots of $BR(\mu \rightarrow e\gamma)$ with running effects due to right-handed neutrinos, as a function of $M_{1/2}$, for different values of $\tan \beta$, and m_0 . Light neutrinos have normal mass ordering with $m_1 = 0.4$ meV. The parameter $|\xi'|$ is chosen as 0.184 in order to maximize the success rate of this model. The horizontal line shows the current MEG bound. For Blue (Red) points the LSP is the lightest neutralino (stau). The percentage in each plot refers to the number of Blue points that satisfy the MEG bound over the total number of points.

trend, the inclusion of the running due to right-handed neutrinos enhances the branching ratio by a factor between about one and two orders of magnitude. The allowed region in the parameter space of the models shrinks, as indicated by the percentage of points that satisfy the current MEG bound. The largest effect occurs for the special A_4 model, also due to the small value $m_1 = 0.4$ meV, which, for normal hierarchy, enhances the contribution in eq. (3.36). In the cases of typical A_4 models and S_4 models, the effect of right-handed neutrinos is similar. Notice that the slope of the plotted regions for $m_0 = 200$ GeV is much steeper than for $m_0 = 5000$ GeV which increases the impact of right-handed neutrinos in the latter case. This is particularly visible in the case of special A_4 models. If we compare the panel (d) of Figs. 11 and 14, where $m_0 = 5000$ GeV and $\tan \beta = 15$, we see that the points are lying on an almost horizontal strip close to the MEG bound and the enhancement due to right-handed neutrinos is sufficient to displace almost all the band above the bound, thus excluding most of the points. In conclusion, running effects due

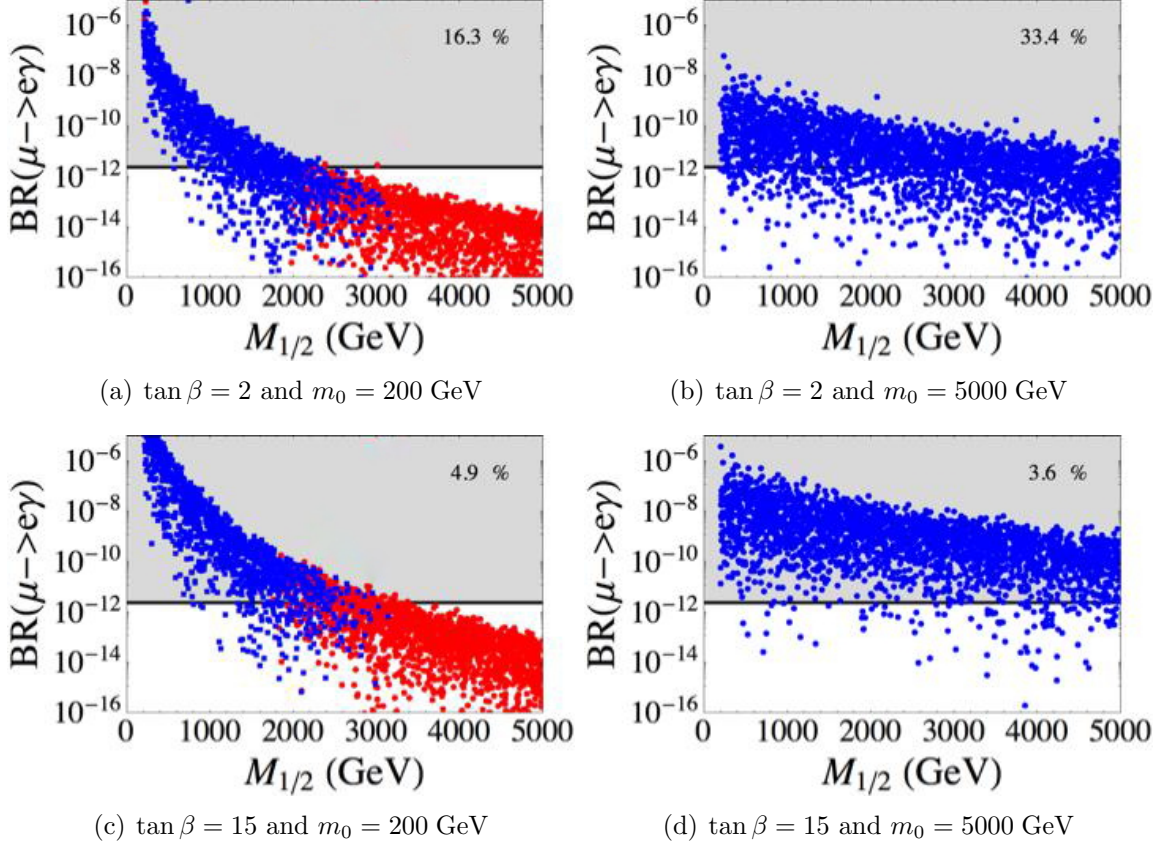


Figure 15: **S_4 Models.** Scatter plots of $BR(\mu \rightarrow e\gamma)$ with running effects due to right-handed neutrinos, as a function of $M_{1/2}$, for different values of $\tan\beta$, and m_0 . Light neutrinos have normal mass ordering with $m_1 = 1$ meV. The parameter ξ is chosen as 0.172 in order to maximize the success rate of this model. The horizontal line shows the current MEG bound. For Blue (Red) points the LSP is the lightest neutralino (stau). The percentage in each plot refers to the number of Blue points that satisfy the MEG bound over the total number of points.

to right-handed neutrinos can significantly contribute to the off-diagonal terms of slepton mass matrices and can even dominate MIs, especially for a pronounced hierarchy in the light neutrino mass spectrum. There is a general reduction in the parameter space of the model and in particular for the special A_4 model with the most hierarchical spectrum. A milder impact is expected for a neutrino mass spectrum close to the degenerate case.

3.4 Correlation with the Muon $g - 2$

The value found for the anomalous magnetic moment of the muon [110]

$$a_\mu^{EXP} = 116592080(63) \times 10^{-11} \quad (3.40)$$

shows a 3.4σ deviation

$$\delta a_\mu = a_\mu^{EXP} - a_\mu^{SM} = +302(88) \times 10^{-11} \quad (3.41)$$

from the value expected in the SM [111–113]

$$a_\mu^{SM} = 116591778(61) \times 10^{-11} . \quad (3.42)$$

It is an interesting question whether the presence of SUSY particles can account for this deviation, once the constraints from the branching ratio of the $\mu \rightarrow e\gamma$ decay are taken into consideration.

Following Refs. [114–117], we study the correlation between δa_μ and $BR(\mu \rightarrow e\gamma)$, for $\tan\beta \in [2, 15]$ and $m_0, M_{1/2} \in [200, 5000]$ GeV, while all the other parameters are treated according to the previous section. Only points corresponding to scenarios with the lightest neutralino being the LSP are shown.

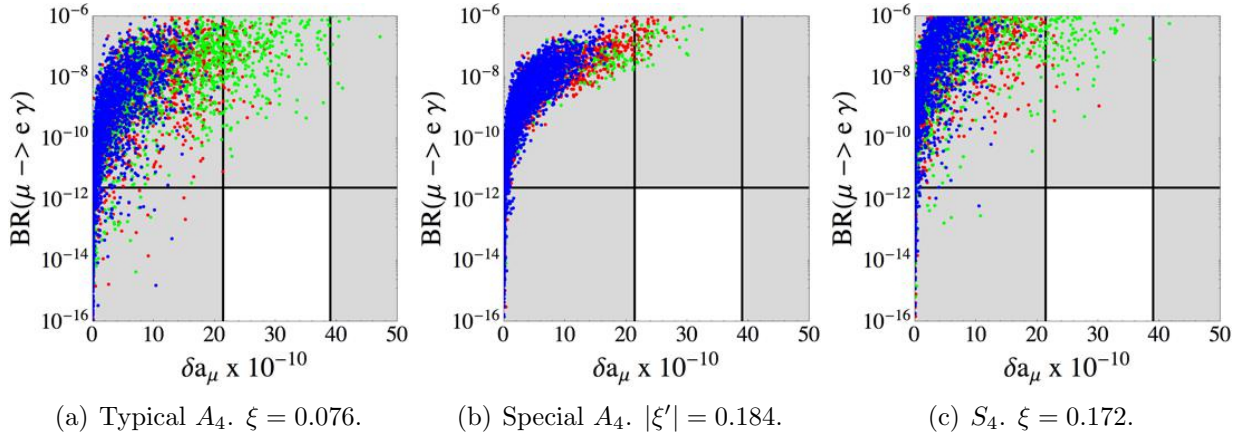


Figure 16: Correlation plots between δa_μ and $BR(\mu \rightarrow e\gamma)$. The value of $\tan\beta$ is taken in the range $[2, 15]$, while $m_0, M_{1/2}$ are chosen between 200 and 5000 GeV. The values of ξ or $|\xi'|$ are those that maximize the success rates for the three models for the NH case. The colour of the points refer to the values of $\tan\beta$: $2 \lesssim \tan\beta \lesssim 7$ in blue, $7 \lesssim \tan\beta \lesssim 11$ in red, $11 \lesssim \tan\beta \lesssim 15$ in green. The horizontal line corresponds to the MEG bound, while the vertical lines correspond to the measurements on δa_μ at 3σ .

As we can see from Fig. 16, in the whole parameter space of the three models it is not natural to reproduce the observed deviation of the muon anomalous magnetic moment, once we consider the present MEG bound on $BR(\mu \rightarrow e\gamma)$. This is not a surprise, because the explanation of the 3.4σ discrepancy needs small values of m_0 and $M_{1/2}$ and larger values of $\tan\beta$, which, however, enhance the branching ratio of the radiative LFV decays.

4 Conclusion

The recent rather precise measurements of θ_{13} make our present knowledge of the neutrino mixing matrix, except for the CP violating phases, sufficiently complete to considerably restrict the class of models that can reproduce the data. In spite of this progress, the range of possibilities for flavour models remains unfortunately quite wide. On the one extreme, the rather large value measured for θ_{13} , close to the old CHOOZ bound, has

validated the prediction of models based on anarchy [118, 119], i.e. no symmetry in the leptonic sector, only chance, so that this possibility remains valid, as discussed, for example, in Ref. [120]. Anarchy can be formulated in a $SU(5) \otimes U(1)$ context by taking different Froggatt-Nielsen [121] charges only for the $SU(5)$ tenplets (for example $10 \sim (3, 2, 0)$, where 3 is the charge of the first generation, 2 of the second, zero of the third) while no charge differences appear in the $\bar{5}$ ($\bar{5} \sim (0, 0, 0)$). Anarchy can be mitigated by assuming that it only holds in the 2-3 sector with the advantage that the first generation masses and the angle θ_{13} are naturally small (see also the recent revisiting in Ref. [122]). In models with See-Saw, one can also play with the charges for the right-handed $SU(5)$ singlet neutrinos. If, for example, one takes $1 \sim (1, -1, 0)$, together with $\bar{5} \sim (2, 0, 0)$, it is possible to get a normal hierarchy model with θ_{13} small and also with $r = \Delta m_{solar}^2 / \Delta m_{atm}^2$ naturally small (see, for example, Ref. [123]). In summary, anarchy and its variants, all based on chance, offer a rather economical class of models that are among those encouraged by the new θ_{13} result. On the other extreme, stimulated by the fact that the data suggest some special mixing patterns as good first approximations (TB or BM, for example), models based on discrete flavour symmetries, like A_4 or S_4 , have been proposed and widely studied. In these models the starting LO approximation is completely fixed (no chance), but the NLO corrections introduce a number of undetermined parameters. The recent data on θ_{13} and the MEG new upper bound on the LFV process $\mu \rightarrow e\gamma$ impose a reappraisal of these models, which we have attempted in this paper. In particular, the relatively large value of θ_{13} introduces a marked departure from the TB limit, while the values of θ_{12} and θ_{23} are very close to it. The challenge is to produce in a natural way a relatively large correction to θ_{13} without affecting too much the other mixing angles. But one must pay attention that these larger corrective terms introduced to shift θ_{13} from the TB value could appear in the non-diagonal elements of the charged lepton (and s-lepton) mass matrix and could induce a too large $\mu \rightarrow e\gamma$ branching ratio.

As a result of our analysis we find that, for reproducing the mixing angles, the Lin type A_4 models have the best performance, as expected, followed by the typical A_4 models, while the BM mixing models lead to an inferior score, as they most often fail to reproduce θ_{12} . In the latter case, if only one complex parameter perturbs the BM pattern, there is a strict correlation among the solar and the reactor angle and the success rate increases considerably by selecting a CP violating Dirac phase close to π .

As for LFV processes we have addressed the problem by adopting the simple CMSSM framework. While this overconstrained version of supersymmetry is rather marginal after the results of the LHC searches, more so if the Higgs mass really is around $m_H = 125$ GeV, we still believe it can be used here for our indicative purposes. We find that the most constrained versions are the models that start with BM mixing at the LO because, in this case, relatively large corrections directly appear in the off-diagonal terms of the charged lepton mass matrix. The typical A_4 models turn out to be the best suited to satisfy the MEG experimental bound, as the non-diagonal charged lepton matrix elements needed to reproduce the mixing angles are quite smaller. An intermediate, still rather good, score is achieved by the models of the Lin type, where the main corrections to the mixing angles arise from the neutrino sector. When the fit to the mixing angles and the bounds on LFV processes are combined, the A_4 models emerge well from our analysis and in particular

those of the Lin type perhaps appear as the most realistic approach to the data among the models based on discrete flavour groups that we have studied. As for the regions of the CMSSM parameter space that are indicated by our analysis the preference is for small $\tan\beta$ and large SUSY masses (at least one out of m_0 and $m_{1/2}$ must be above 1 TeV). As a consequence it appears impossible, at least within the CMSSM model, to satisfy the MEG bound and, at the same time, to reproduce the muon $g - 2$ discrepancy.

Acknowledgements

We recognize that this work has been partly supported by the Italian Ministero dell'Università e della Ricerca Scientifica, under the COFIN program (PRIN 2008), by the European Commission, under the networks ‘‘Heptools’’, ‘‘Quest for Unification’’, ‘‘LHCPHENONET’’ and European Union FP7 ITN INVISIBLES (Marie Curie Actions, PITN-GA-2011-289442) and contracts MRTN-CT-2006-035505 and PITN-GA-2009-237920 (UNILHC), and by the Technische Universität München – Institute for Advanced Study, funded by the German Excellence Initiative.

A Expression of $a_{CC'}$

In this section we list the explicit expression of $a_{CC'}$ in our conventions:

$$\begin{aligned}
a_{LL} &= \frac{g^2}{16\pi^2} \left[f_{1n}(a_2) + f_{1c}(a_2) + \frac{M_2\mu \tan\beta}{M_2^2 - \mu^2} \left(f_{2n}(a_2, b) + f_{2c}(a_2, b) \right) \right. \\
&\quad \left. + \tan^2\theta_W \left(f_{1n}(a_1) - \frac{M_1\mu \tan\beta}{M_1^2 - \mu^2} f_{2n}(a_1, b) - M_1 (m_{SUSY} - \mu \tan\beta) \frac{f_{3n}(a_1)}{m_{SUSY}^2} \right) \right] \\
a_{RL} &= \frac{g^2}{16\pi^2} \tan^2\theta_W \frac{M_1}{m_{SUSY}} 2f_{2n}(a_1) \\
a_{RR} &= \frac{g^2}{16\pi^2} \tan^2\theta_W \left[4f_{1n}(a_1) + 2 \frac{M_1\mu \tan\beta}{M_1^2 - \mu^2} f_{2n}(a_1, b) - M_1 (m_{SUSY} - \mu \tan\beta) \frac{f_{3n}(a_1)}{m_{SUSY}^2} \right] \\
a_{LR} &= \frac{g^2}{16\pi^2} \tan^2\theta_W \frac{M_1}{m_{SUSY}} 2f_{2n}(a_1)
\end{aligned} \tag{A.1}$$

where $a_{1,2} = M_{1,2}^2/m_{SUSY}^2$, $b = \mu^2/m_{SUSY}^2$ and $f_{i(c,n)}(x, y) = f_{i(c,n)}(x) - f_{i(c,n)}(y)$. The functions $f_{in}(x)$ and $f_{ic}(x)$, slightly different from those in Ref. [124], are given by:

$$\begin{aligned}
f_{1n}(x) &= (-17x^3 + 9x^2 + 9x - 1 + 6x^2(x+3)\log x)/(24(1-x)^5) \\
f_{2n}(x) &= (-5x^2 + 4x + 1 + 2x(x+2)\log x)/(4(1-x)^4) \\
f_{3n}(x) &= (1 + 9x - 9x^2 - x^3 + 6x(x+1)\log x)/(2(1-x)^5) \\
f_{1c}(x) &= (-x^3 - 9x^2 + 9x + 1 + 6x(x+1)\log x)/(6(1-x)^5) \\
f_{2c}(x) &= (-x^2 - 4x + 5 + 2(2x+1)\log x)/(2(1-x)^4).
\end{aligned} \tag{A.2}$$

References

- [1] G. Altarelli and F. Feruglio, *Models of Neutrino Masses and Mixings*, New J. Phys. **6** (2004) 106, [[hep-ph/0405048](#)].
- [2] R. N. Mohapatra and A. Y. Smirnov, *Neutrino Mass and New Physics*, Ann. Rev. Nucl. Part. Sci. **56** (2006) 569–628, [[hep-ph/0603118](#)].
- [3] W. Grimus, *Neutrino physics: Models for neutrino masses and lepton mixing*, PoS **P2GC** (2006) 001, [[hep-ph/0612311](#)].
- [4] M. C. Gonzalez-Garcia and M. Maltoni, *Phenomenology with Massive Neutrinos*, Phys. Rept. **460** (2008) 1–129, [[arXiv:0704.1800](#)].
- [5] G. Altarelli, *Status of Neutrino Masses and Mixing in 2009*, Nuovo Cim. **C32N5-6** (2009) 91–102, [[arXiv:0905.3265](#)].
- [6] G. Altarelli, *Status of Neutrino Masses and Mixing in 2010*, PoS **HRMS²010** (2010) 022, [[arXiv:1011.5342](#)].
- [7] G. Fogli, E. Lisi, A. Marrone, D. Montanino, A. Palazzo, *et. al.*, *Global Analysis of Neutrino Masses, Mixings and Phases: Entering the Era of Leptonic CP Violation Searches*, [arXiv:1205.5254](#).
- [8] M. Tortola, J. Valle, and D. Vanegas, *Global Status of Neutrino Oscillation Parameters After Recent Reactor Measurements*, [arXiv:1205.4018](#).
- [9] **T2K** Collaboration, K. Abe *et. al.*, *Indication of Electron Neutrino Appearance from an Accelerator-Produced Off-Axis Muon Neutrino Beam*, Phys. Rev. Lett. **107** (2011) 041801, [[arXiv:1106.2822](#)].
- [10] **MINOS** Collaboration, P. Adamson *et. al.*, *Improved search for muon-neutrino to electron-neutrino oscillations in MINOS*, Phys. Rev. Lett. **107** (2011) 181802, [[arXiv:1108.0015](#)].
- [11] **DOUBLE-CHOOZ** Collaboration, Y. Abe *et. al.*, *Indication for the Disappearance of Reactor Electron Antineutrinos in the Double Chooz Experiment*, [arXiv:1112.6353](#).
- [12] **DAYA-BAY** Collaboration, F. P. An *et. al.*, *Observation of Electron-Antineutrino Disappearance at Daya Bay*, [arXiv:1203.1669](#).
- [13] **RENO** Collaboration, J. K. Ahn *et. al.*, *Observation of Reactor Electron Antineutrino Disappearance in the Reno Experiment*, [arXiv:1204.0626](#).
- [14] G. Altarelli and F. Feruglio, *Discrete Flavor Symmetries and Models of Neutrino Mixing*, Rev. Mod. Phys. **82** (2010) 2701–2729, [[arXiv:1002.0211](#)].
- [15] H. Ishimori *et. al.*, *Non-Abelian Discrete Symmetries in Particle Physics*, Prog. Theor. Phys. Suppl. **183** (2010) 1–163, [[arXiv:1003.3552](#)].

- [16] P. O. Ludl, *On the Finite Subgroups of $U(3)$ of Order Smaller Than 512*, J. Phys. **A43** (2010) 395204, [[arXiv:1006.1479](#)].
- [17] W. Grimus and P. O. Ludl, *Principal Series of Finite Subgroups of $SU(3)$* , J. Phys. **A43** (2010) 445209, [[arXiv:1006.0098](#)].
- [18] K. M. Parattu and A. Wingerter, *Tribimaximal Mixing from Small Groups*, Phys. Rev. **D84** (2011) 013011, [[arXiv:1012.2842](#)].
- [19] W. Grimus and P. O. Ludl, *Finite Flavour Groups of Fermions*, [arXiv:1110.6376](#).
- [20] P. F. Harrison, D. H. Perkins, and W. G. Scott, *Tri-Bimaximal Mixing and the Neutrino Oscillation Data*, Phys. Lett. **B530** (2002) 167, [[hep-ph/0202074](#)].
- [21] P. F. Harrison and W. G. Scott, *Symmetries and Generalisations of Tri-Bimaximal Neutrino Mixing*, Phys. Lett. **B535** (2002) 163–169, [[hep-ph/0203209](#)].
- [22] Z.-z. Xing, *Nearly Tri-Bimaximal Neutrino Mixing and CP Violation*, Phys. Lett. **B533** (2002) 85–93, [[hep-ph/0204049](#)].
- [23] P. F. Harrison and W. G. Scott, *Mu - Tau Reflection Symmetry in Lepton Mixing and Neutrino Oscillations*, Phys. Lett. **B547** (2002) 219–228, [[hep-ph/0210197](#)].
- [24] P. F. Harrison and W. G. Scott, *Permutation Symmetry, Tri-Bimaximal Neutrino Mixing and the S^3 Group Characters*, Phys. Lett. **B557** (2003) 76, [[hep-ph/0302025](#)].
- [25] Y. Kajiyama, M. Raidal, and A. Strumia, *The Golden Ratio Prediction for the Solar Neutrino Mixing*, Phys. Rev. **D76** (2007) 117301, [[arXiv:0705.4559](#)].
- [26] L. L. Everett and A. J. Stuart, *Icosahedral (A_5) Family Symmetry and the Golden Ratio Prediction for Solar Neutrino Mixing*, Phys. Rev. **D79** (2009) 085005, [[arXiv:0812.1057](#)].
- [27] G.-J. Ding, L. L. Everett, and A. J. Stuart, *Golden Ratio Neutrino Mixing and A_5 Flavor Symmetry*, Nucl. Phys. **B857** (2012) 219–253, [[arXiv:1110.1688](#)].
- [28] F. Feruglio and A. Paris, *The Golden Ratio Prediction for the Solar Angle from a Natural Model with A_5 Flavour Symmetry*, JHEP **03** (2011) 101, [[arXiv:1101.0393](#)].
- [29] W. Rodejohann, *Unified Parametrization for Quark and Lepton Mixing Angles*, Phys. Lett. **B671** (2009) 267–271, [[arXiv:0810.5239](#)].
- [30] A. Adulpravitchai, A. Blum, and W. Rodejohann, *Golden Ratio Prediction for Solar Neutrino Mixing*, New J. Phys. **11** (2009) 063026, [[arXiv:0903.0531](#)].
- [31] G. Altarelli, F. Feruglio, and I. Masina, *Can Neutrino Mixings Arise from the Charged Lepton Sector?*, Nucl. Phys. **B689** (2004) 157–171, [[hep-ph/0402155](#)].

- [32] M. Raidal, *Relation Between the Neutrino and Quark Mixing Angles and Grand Unification*, Phys. Rev. Lett. **93** (2004) 161801, [[hep-ph/0404046](#)].
- [33] H. Minakata and A. Y. Smirnov, *Neutrino Mixing and Quark-Lepton Complementarity*, Phys. Rev. **D70** (2004) 073009, [[hep-ph/0405088](#)].
- [34] P. H. Frampton and R. N. Mohapatra, *Possible Gauge Theoretic Origin for Quark-Lepton Complementarity*, JHEP **01** (2005) 025, [[hep-ph/0407139](#)].
- [35] J. Ferrandis and S. Pakvasa, *QLC Relation and Neutrino Mass Hierarchy*, Phys. Rev. **D71** (2005) 033004, [[hep-ph/0412038](#)].
- [36] S. K. Kang, C. S. Kim, and J. Lee, *Quark-Lepton Complementarity with Renormalization Effects Through Threshold Corrections*, Phys. Lett. **B619** (2005) 129–135, [[hep-ph/0501029](#)].
- [37] N. Li and B.-Q. Ma, *Unified Parametrization of Quark and Lepton Mixing Matrices*, Phys. Rev. **D71** (2005) 097301, [[hep-ph/0501226](#)].
- [38] K. Cheung, S. K. Kang, C. S. Kim, and J. Lee, *Lepton Flavor Violation as a Probe of Quark-Lepton Unification*, Phys. Rev. **D72** (2005) 036003, [[hep-ph/0503122](#)].
- [39] Z.-z. Xing, *Nontrivial Correlation Between the CKM and MNS Matrices*, Phys. Lett. **B618** (2005) 141–149, [[hep-ph/0503200](#)].
- [40] A. Datta, L. Everett, and P. Ramond, *Cabibbo Haze in Lepton Mixing*, Phys. Lett. **B620** (2005) 42–51, [[hep-ph/0503222](#)].
- [41] S. Antusch, S. F. King, and R. N. Mohapatra, *Quark Lepton Complementarity in Unified Theories*, Phys. Lett. **B618** (2005) 150–161, [[hep-ph/0504007](#)].
- [42] M. Lindner, M. A. Schmidt, and A. Y. Smirnov, *Screening of Dirac Flavor Structure in the Seesaw and Neutrino Mixing*, JHEP **07** (2005) 048, [[hep-ph/0505067](#)].
- [43] H. Minakata, *Quark-Lepton Complementarity: a Review*, [hep-ph/0505262](#).
- [44] T. Ohlsson, *Bimaximal Fermion Mixing from the Quark and Leptonic Mixing Matrices*, Phys. Lett. **B622** (2005) 159–164, [[hep-ph/0506094](#)].
- [45] S. F. King, *Predicting Neutrino Parameters from $SO(3)$ Family Symmetry and Quark-Lepton Unification*, JHEP **08** (2005) 105, [[hep-ph/0506297](#)].
- [46] A. Dighe, S. Goswami, and P. Roy, *Quark-Lepton Complementarity with Quasidegenerate Majorana Neutrinos*, Phys. Rev. **D73** (2006) 071301, [[hep-ph/0602062](#)].
- [47] B. C. Chauhan, M. Picariello, J. Pulido, and E. Torrente-Lujan, *Quark-Lepton Complementarity, Neutrino and Standard Model Data Predict $(\theta_{13}^{PMNS} = 9_{-2}^{+1})^\circ$* , Eur. Phys. J. **C50** (2007) 573–578, [[hep-ph/0605032](#)].

- [48] K. A. Hochmuth and W. Rodejohann, *Low and High Energy Phenomenology of Quark-Lepton Complementarity Scenarios*, Phys. Rev. **D75** (2007) 073001, [[hep-ph/0607103](#)].
- [49] M. A. Schmidt and A. Y. Smirnov, *Quark Lepton Complementarity and Renormalization Group Effects*, Phys. Rev. **D74** (2006) 113003, [[hep-ph/0607232](#)].
- [50] F. Plentinger, G. Seidl, and W. Winter, *Systematic Parameter Space Search of Extended Quark-Lepton Complementarity*, Nucl. Phys. **B791** (2008) 60–92, [[hep-ph/0612169](#)].
- [51] F. Plentinger, G. Seidl, and W. Winter, *The Seesaw Mechanism in Quark-Lepton Complementarity*, Phys. Rev. **D76** (2007) 113003, [[arXiv:0707.2379](#)].
- [52] G. Altarelli, F. Feruglio, and L. Merlo, *Revisiting Bimaximal Neutrino Mixing in a Model with S_4 Discrete Symmetry*, JHEP **05** (2009) 020, [[arXiv:0903.1940](#)].
- [53] R. de Adelhart Toorop, F. Bazzocchi, and L. Merlo, *The Interplay Between GUT and Flavour Symmetries in a Pati-Salam $\times S_4$ Model*, JHEP **08** (2010) 001, [[arXiv:1003.4502](#)].
- [54] K. M. Patel, *An $SO(10) \times S_4$ Model of Quark-Lepton Complementarity*, Phys. Lett. **B695** (2011) 225–230, [[arXiv:1008.5061](#)].
- [55] D. Meloni, *Bimaximal mixing and large θ_{13} in a SUSY $SU(5)$ model based on S_4* , JHEP **10** (2011) 010, [[arXiv:1107.0221](#)].
- [56] Y. Shimizu and R. Takahashi, *Deviations from Tri-Bimaximality and Quark-Lepton Complementarity*, Europhys.Lett. **93** (2011) 61001, [[arXiv:1009.5504](#)].
- [57] Y. H. Ahn, H.-Y. Cheng, and S. Oh, *Quark-Lepton Complementarity and Tribimaximal Neutrino Mixing from Discrete Symmetry*, Phys. Rev. **D83** (2011) 076012, [[arXiv:1102.0879](#)].
- [58] I. d. M. Varzielas and G. G. Ross, *Discrete Family Symmetry, Higgs Mediators and θ_{13}* , [[arXiv:1203.6636](#)].
- [59] C. Hagedorn and M. Serone, *Leptons in Holographic Composite Higgs Models with Non-Abelian Discrete Symmetries*, JHEP **1110** (2011) 083, [[arXiv:1106.4021](#)].
- [60] C. Hagedorn and M. Serone, *General Lepton Mixing in Holographic Composite Higgs Models*, JHEP **1202** (2012) 077, [[arXiv:1110.4612](#)].
- [61] Y. Lin, *Tri-Bimaximal Neutrino Mixing from A_4 and $\theta_{13} \sim \theta_C$* , Nucl. Phys. **B824** (2010) 95–110, [[arXiv:0905.3534](#)].
- [62] I. de Medeiros Varzielas and L. Merlo, *Ultraviolet Completion of Flavour Models*, JHEP **02** (2011) 062, [[arXiv:1011.6662](#)].

- [63] L. Calibbi, Z. Lalak, S. Pokorski, and R. Ziegler, *Universal Constraints on Low-Energy Flavour Models*, [arXiv:1204.1275](#).
- [64] **MEG** Collaboration, J. Adam *et. al.*, *New Limit on the Lepton-Flavour Violating Decay $\mu \rightarrow e\gamma$* , [arXiv:1107.5547](#).
- [65] R. d. A. Toorop, F. Feruglio, and C. Hagedorn, *Discrete Flavour Symmetries in Light of T2K*, Phys. Lett. **B703** (2011) 447–451, [[arXiv:1107.3486](#)].
- [66] R. de Adelhart Toorop, F. Feruglio, and C. Hagedorn, *Finite Modular Groups and Lepton Mixing*, Nucl. Phys. **B858** (2012) 437–467, [[arXiv:1112.1340](#)].
- [67] S.-F. Ge, D. A. Dicus, and W. W. Repko, *Z_2 Symmetry Prediction for the Leptonic Dirac CP Phase*, Phys.Lett. **B702** (2011) 220–223, [[arXiv:1104.0602](#)].
- [68] S.-F. Ge, D. A. Dicus, and W. W. Repko, *Residual Symmetries for Neutrino Mixing with a Large θ_{13} and Nearly Maximal δ_D* , Phys.Rev.Lett. **108** (2012) 041801, [[arXiv:1108.0964](#)].
- [69] D. Hernandez and A. Y. Smirnov, *Lepton Mixing and Discrete Symmetries*, [arXiv:1204.0445](#).
- [70] G. Altarelli and F. Feruglio, *Tri-Bimaximal Neutrino Mixing from Discrete Symmetry in Extra Dimensions*, Nucl. Phys. **B720** (2005) 64–88, [[hep-ph/0504165](#)].
- [71] G. Altarelli and F. Feruglio, *Tri-Bimaximal Neutrino Mixing, A_4 and the Modular Symmetry*, Nucl. Phys. **B741** (2006) 215–235, [[hep-ph/0512103](#)].
- [72] G. Altarelli and D. Meloni, *A Simplest A_4 Model for Tri-Bimaximal Neutrino Mixing*, J. Phys. **G36** (2009) 085005, [[arXiv:0905.0620](#)].
- [73] F. Bazzocchi, L. Merlo, and S. Morisi, *Fermion Masses and Mixings in a S_4 -Based Model*, Nucl. Phys. **B816** (2009) 204–226, [[arXiv:0901.2086](#)].
- [74] F. Bazzocchi, L. Merlo, and S. Morisi, *Phenomenological Consequences of See-Saw in S_4 Based Models*, Phys. Rev. **D80** (2009) 053003, [[arXiv:0902.2849](#)].
- [75] G.-J. Ding, *Fermion Masses and Flavor Mixings in a Model with S_4 Flavor Symmetry*, Nucl. Phys. **B827** (2010) 82–111, [[arXiv:0909.2210](#)].
- [76] D. Meloni, *A See-Saw S_4 Model for Fermion Masses and Mixings*, J. Phys. **G37** (2010) 055201, [[arXiv:0911.3591](#)].
- [77] F. Feruglio, C. Hagedorn, Y. Lin, and L. Merlo, *Tri-Bimaximal Neutrino Mixing and Quark Masses from a Discrete Flavour Symmetry*, Nucl. Phys. **B775** (2007) 120–142, [[hep-ph/0702194](#)].
- [78] S. F. King, *Parametrizing the Lepton Mixing Matrix in Terms of Deviations from Tri-Bimaximal Mixing*, Phys. Lett. **B659** (2008) 244–251, [[arXiv:0710.0530](#)].

- [79] L. J. Hall, V. A. Kostelecky, and S. Raby, *New Flavor Violations in Supergravity Models*, Nucl. Phys. **B267** (1986) 415.
- [80] I. Masina and C. A. Savoy, *Sleptonarium (Constraints on the CP and Flavour Pattern of Scalar Lepton Masses)*, Nucl. Phys. **B661** (2003) 365–393, [[hep-ph/0211283](#)].
- [81] P. Paradisi, *Constraints on SUSY Lepton Flavour Violation by Rare Processes*, JHEP **10** (2005) 006, [[hep-ph/0505046](#)].
- [82] J. Hisano, T. Moroi, K. Tobe, M. Yamaguchi, and T. Yanagida, *Lepton Flavor Violation in the Supersymmetric Standard Model with Seesaw Induced Neutrino Masses*, Phys. Lett. **B357** (1995) 579–587, [[hep-ph/9501407](#)].
- [83] J. Hisano, T. Moroi, K. Tobe, and M. Yamaguchi, *Lepton-Flavor Violation via Right-Handed Neutrino Yukawa Couplings in Supersymmetric Standard Model*, Phys. Rev. **D53** (1996) 2442–2459, [[hep-ph/9510309](#)].
- [84] J. Hisano and K. Tobe, *Neutrino Masses, Muon $G-2$, and Lepton-Flavour Violation in the Supersymmetric See-Saw Model*, Phys. Lett. **B510** (2001) 197–204, [[hep-ph/0102315](#)].
- [85] T. Fukuyama, A. Ilakovac, and T. Kikuchi, *Lepton Flavour Violating Leptonic / Semileptonic Decays of Charged Leptons in the Minimal Supersymmetric Standard Model*, Eur. Phys. J. **C56** (2008) 125–146, [[hep-ph/0506295](#)].
- [86] E. Arganda and M. J. Herrero, *Testing Supersymmetry with Lepton Flavor Violating Tau and Mu Decays*, Phys. Rev. **D73** (2006) 055003, [[hep-ph/0510405](#)].
- [87] G. Isidori, F. Mescia, P. Paradisi, and D. Temes, *Flavour Physics at Large $\tan(\beta)$ with a Bino-Like LSP*, Phys. Rev. **D75** (2007) 115019, [[hep-ph/0703035](#)].
- [88] M. Endo and T. Shindou, *Lepton-Flavour Violation in the Light of Leptogenesis and Muon $g - 2$* , [arXiv:0805.0996](#).
- [89] K. Hamaguchi, M. Kakizaki, and M. Yamaguchi, *Democratic (S)Fermions and Lepton Flavor Violation*, Phys. Rev. **D68** (2003) 056007, [[hep-ph/0212172](#)].
- [90] A. Mondragon, M. Mondragon, and E. Peinado, *Lepton Masses, Mixings and FCNC in a Minimal S_3 -Invariant Extension of the Standard Model*, Phys. Rev. **D76** (2007) 076003, [[arXiv:0706.0354](#)].
- [91] N. Kifune, J. Kubo, and A. Lenz, *Flavor Changing Neutral Higgs Bosons in a Supersymmetric Extension Based on a $Q(6)$ Family Symmetry*, Phys. Rev. **D77** (2008) 076010, [[arXiv:0712.0503](#)].
- [92] H. Ishimori *et al.*, *Soft Supersymmetry Breaking Terms from $D_4 \times Z_2$ Lepton Flavor Symmetry*, Phys. Rev. **D77** (2008) 115005, [[arXiv:0803.0796](#)].

- [93] F. Feruglio, C. Hagedorn, Y. Lin, and L. Merlo, *Lepton Flavour Violation in Models with A_4 Flavour Symmetry*, Nucl. Phys. **B809** (2009) 218–243, [[arXiv:0807.3160](#)].
- [94] H. Ishimori, T. Kobayashi, Y. Omura, and M. Tanimoto, *Soft Supersymmetry Breaking Terms from A_4 Lepton Flavor Symmetry*, JHEP **12** (2008) 082, [[arXiv:0807.4625](#)].
- [95] H. Ishimori, T. Kobayashi, H. Okada, Y. Shimizu, and M. Tanimoto, *$\Delta(54)$ Flavor Model for Leptons and Sleptons*, JHEP **12** (2009) 054, [[arXiv:0907.2006](#)].
- [96] F. Feruglio, C. Hagedorn, and L. Merlo, *Vacuum Alignment in SUSY A_4 Models*, JHEP **03** (2010) 084, [[arXiv:0910.4058](#)].
- [97] F. Feruglio, C. Hagedorn, Y. Lin, and L. Merlo, *Lepton Flavour Violation in a Supersymmetric Model with A_4 Flavour Symmetry*, Nucl. Phys. **B832** (2010) 251–288, [[arXiv:0911.3874](#)].
- [98] C. Hagedorn, E. Molinaro, and S. T. Petcov, *Charged Lepton Flavour Violating Radiative Decays $\ell_i \rightarrow \ell_j + \gamma$ in See-Saw Models with A_4 Symmetry*, JHEP **02** (2010) 047, [[arXiv:0911.3605](#)].
- [99] L. Merlo, S. Rigolin, and B. Zaldivar, *Flavour Violation in a Supersymmetric T' Model*, JHEP **11** (2011) 047, [[arXiv:1108.1795](#)].
- [100] J. Chakraborty, P. Ghosh, and W. Rodejohann, *Lower Limits on $\mu \rightarrow e\gamma$ from New Measurements on U_{e3}* , [arXiv:1204.1000](#).
- [101] G. G. Ross and O. Vives, *Yukawa Structure, Flavour and CP Violation in Supergravity*, Phys. Rev. **D67** (2003) 095013, [[hep-ph/0211279](#)].
- [102] S. Antusch, S. F. King, M. Malinsky, and G. G. Ross, *Solving the SUSY Flavour and CP Problems with Non-Abelian Family Symmetry and Supergravity*, Phys. Lett. **B670** (2009) 383–389, [[arXiv:0807.5047](#)].
- [103] V. Cirigliano, B. Grinstein, G. Isidori, and M. B. Wise, *Minimal flavor violation in the lepton sector*, Nucl. Phys. **B728** (2005) 121–134, [[hep-ph/0507001](#)].
- [104] S. Davidson and F. Palorini, *Various Definitions of Minimal Flavour Violation for Leptons*, Phys. Lett. **B642** (2006) 72–80, [[hep-ph/0607329](#)].
- [105] B. Grinstein, V. Cirigliano, G. Isidori, and M. B. Wise, *Grand Unification and the Principle of Minimal Flavor Violation*, Nucl. Phys. **B763** (2007) 35–48, [[hep-ph/0608123](#)].
- [106] R. Alonso, G. Isidori, L. Merlo, L. A. Munoz, and E. Nardi, *Minimal Flavour Violation Extensions of the Seesaw*, JHEP **06** (2011) 037, [[arXiv:1103.5461](#)].
- [107] F. Borzumati and A. Masiero, *Large Muon and Electron Number Violations in Supergravity Theories*, Phys. Rev. Lett. **57** (1986) 961.

- [108] F. Gabbiani and A. Masiero, *FCNC in Generalized Supersymmetric Theories*, Nucl. Phys. **B322** (1989) 235.
- [109] S. T. Petcov, S. Profumo, Y. Takanishi, and C. E. Yaguna, *Charged Lepton Flavor Violating Decays: Leading Logarithmic Approximation Versus Full RG Results*, Nucl. Phys. **B676** (2004) 453–480, [[hep-ph/0306195](#)].
- [110] **Muon G-2** Collaboration, G. W. Bennett *et. al.*, *Final Report of the Muon E821 Anomalous Magnetic Moment Measurement at Bnl*, Phys. Rev. **D73** (2006) 072003, [[hep-ex/0602035](#)].
- [111] K. Hagiwara, A. D. Martin, D. Nomura, and T. Teubner, *Improved Predictions for $g - 2$ of the Muon and $\alpha_{\text{QED}}(M_Z^2)$* , Phys. Lett. **B649** (2007) 173–179, [[hep-ph/0611102](#)].
- [112] M. Passera, W. J. Marciano, and A. Sirlin, *The Muon $g - 2$ and the Bounds on the Higgs Boson Mass*, Phys. Rev. **D78** (2008) 013009, [[arXiv:0804.1142](#)].
- [113] M. Passera, W. J. Marciano, and A. Sirlin, *The Muon $g - 2$ Discrepancy: Errors Or New Physics?*, AIP Conf. Proc. **1078** (2009) 378–381, [[arXiv:0809.4062](#)].
- [114] T. Moroi, *The Muon Anomalous Magnetic Dipole Moment in the Minimal Supersymmetric Standard Model*, Phys. Rev. **D53** (1996) 6565–6575, [[hep-ph/9512396](#)].
- [115] S. P. Martin and J. D. Wells, *Muon Anomalous Magnetic Dipole Moment in Supersymmetric Theories*, Phys. Rev. **D64** (2001) 035003, [[hep-ph/0103067](#)].
- [116] D. Stockinger, *The Muon Magnetic Moment and Supersymmetry*, J. Phys. **G34** (2007) R45–R92, [[hep-ph/0609168](#)].
- [117] A. Czarnecki and W. J. Marciano, *The Muon Anomalous Magnetic Moment: a Harbinger for ‘New Physics’*, Phys. Rev. **D64** (2001) 013014, [[hep-ph/0102122](#)].
- [118] L. J. Hall, H. Murayama, and N. Weiner, *Neutrino Mass Anarchy*, Phys. Rev. Lett. **84** (2000) 2572–2575, [[hep-ph/9911341](#)].
- [119] A. de Gouvea and H. Murayama, *Statistical Test of Anarchy*, Phys. Lett. **B573** (2003) 94–100, [[hep-ph/0301050](#)].
- [120] A. de Gouvea and H. Murayama, *Neutrino Mixing Anarchy: Alive and Kicking*, [arXiv:1204.1249](#).
- [121] C. D. Froggatt and H. B. Nielsen, *Hierarchy of Quark Masses, Cabibbo Angles and CP Violation*, Nucl. Phys. **B147** (1979) 277.
- [122] W. Buchmuller, V. Domeke, and K. Schmitz, *Predicting θ_{13} and the Neutrino Mass Scale from Quark Lepton Mass Hierarchies*, JHEP **03** (2012) 008, [[arXiv:1111.3872](#)].

- [123] G. Altarelli, F. Feruglio, and I. Masina, *Models of Neutrino Masses: Anarchy Versus Hierarchy*, JHEP **01** (2003) 035, [[hep-ph/0210342](#)].
- [124] M. Ciuchini *et. al.*, *Soft SUSY Breaking Grand Unification: Leptons Versus Quarks on the Flavor Playground*, Nucl. Phys. **B783** (2007) 112–142, [[hep-ph/0702144](#)].